



**The University of Sydney**

School of Civil Engineering  
Sydney NSW 2006  
AUSTRALIA

<http://www.civil.usyd.edu.au/>

Centre for Advanced Structural Engineering

**Interaction Buckling and Postbuckling in  
the Distortional Mode of Thin-Walled  
Sections**

**Research Report No R870**

**Derrick C Y Yap BE  
Gregory J Hancock BSc BE PhD DEng**

**April 2006**

ISSN 1833-2781



The University of Sydney

School of Civil Engineering  
Centre for Advanced Structural Engineering  
<http://www.civil.usyd.edu.au/>

## Interaction Buckling and Postbuckling in the Distortional Mode of Thin-Walled Sections

Research Report No R870

Derrick C Y Yap, BE  
Gregory J Hancock, BSc, BE, PhD, DEng

April 2006

### Abstract:

The buckling modes of cold-formed thin-walled sections with edge stiffeners are generally in the forms of the short half-wavelength local buckle, the intermediate half-wavelength distortional buckle and the long half-wavelength flexural/flexural-torsional buckle. These buckling modes usually occur at distinct lengths. However the possibility of the interaction of buckling modes may be present at certain lengths. This may be due to the distortional mode interacting with the local buckling mode, both of which may be in the post-buckling range.

Local buckling has been well researched and accounted for in design standards with an effective width model developed by Von Karman et al (1932) to produce a simple model of the post-buckling reserve strength. Distortional buckling research has made much headway in recent years at the University of Sydney by Hancock (1985), Lau and Hancock (1990), Kwon and Hancock (1992) and Yang and Hancock (2004), at Johns Hopkins University by Schafer (2002) and the Technical University of Lisbon, Portugal by Silvestre and Camotim (2004). What has been known for some time is that the distortional mode has a post-buckling reserve strength which is generally less than that of local buckling. However, the nature of this post-buckling reserve is not clearly understood, particularly what precipitates failure.

Some research has been done to understand the buckling mode interaction of local and distortional. This is usually carried out by analytically separating the combined modes into its composition of individual modes. Generalised Beam Theory (GBT) uses explicit analytical expressions to analyse the influence of local and distortional buckling modes. Another method currently being developed is modal identification and decomposition, where a numerical method is employed to calculate the critical loads for the pure buckling modes.

The paper discusses the analysis of post-buckling in the distortional mode of a thin-walled section with edge stiffeners and the effect of interaction of buckling modes on failure loads. The analysis is based on the longitudinal stress development and redistribution using the finite element package ABAQUS. This methodology whereby the longitudinal stress redistribution is studied is similar to the work of Von Karman et al, in predicting the post-local buckling behaviour.

### Keywords:

Stress distribution; local buckling; distortional buckling; interaction buckling; postbuckling behaviour; finite element analysis

**Copyright Notice****School of Civil Engineering, Research Report R870****Interaction Buckling and Postbuckling in the Distortional Mode of Thin-Walled Sections**

© 2006 Derrick C. Y. Yap & Gregory J. Hancock

Email: [D.Yap@civil.usyd.edu.au](mailto:D.Yap@civil.usyd.edu.au)  
[hancock@eng.usyd.edu.au](mailto:hancock@eng.usyd.edu.au)

ISSN 1833-2781

This publication may be redistributed freely in its entirety and in its original form without the consent of the copyright owner.

Use of material contained in this publication in any other published works must be appropriately referenced, and, if necessary, permission sought from the author.

Published by:  
School of Civil Engineering  
The University of Sydney  
Sydney NSW 2006  
AUSTRALIA

April 2006

This report and other Research Reports published by The School of Civil Engineering are available on the Internet:

<http://www.civil.usyd.edu.au>

# TABLE OF CONTENTS

<b>TABLE OF CONTENTS</b> .....	<b>3</b>
<b>1 INTRODUCTION</b> .....	<b>5</b>
<b>2 SECTIONS INVESTIGATED</b> .....	<b>5</b>
<b>3 FINITE ELEMENT ANALYSIS</b> .....	<b>6</b>
3.1 GENERAL .....	6
3.2 TYPE OF ELEMENT AND FINITE ELEMENT MESH .....	7
3.3 BOUNDARY CONDITIONS AND METHOD OF LOADING.....	7
3.4 MATERIAL PROPERTIES AND MATERIAL ORIENTATION.....	7
3.5 GEOMETRIC IMPERFECTIONS.....	8
3.6 ANALYSES .....	8
3.6.1 <i>Eigenvalue buckling analysis</i> .....	8
3.6.2 <i>Postbuckling analysis</i> .....	9
<b>4 SENSITIVITY AND VALIDATION ANALYSES</b> .....	<b>9</b>
<b>5 POSTBUCKLING BEHAVIOUR</b> .....	<b>11</b>
5.1 LOAD DEFLECTION CURVES .....	12
5.2 LONGITUDINAL STRESS DISTRIBUTIONS .....	12
5.2.1 <i>Section with 6 mm thickness</i> .....	12
5.2.2 <i>Section with 3 mm thickness</i> .....	13
5.2.3 <i>Section with 1 mm thickness</i> .....	14
<b>6 TEST RESULTS IN RELATION TO STRENGTH DESIGN CURVES WITH 0.5 AND 0.6 COEFFICIENTS</b> .....	<b>16</b>
<b>7 CONCLUSION</b> .....	<b>16</b>
<b>ACKNOWLEDGEMENTS</b> .....	<b>18</b>
<b>REFERENCES</b> .....	<b>19</b>
<b>NOTATIONS</b> .....	<b>21</b>
<b>FIGURES</b> .....	<b>22</b>
<b>TABLES</b> .....	<b>38</b>



# 1 INTRODUCTION

Thin-walled sections such as lipped channels can buckle in three different modes being the short half-wavelength local buckle, the intermediate half-wavelength distortional buckle and the long half-wavelength flexural/flexural-torsional buckle (Hancock, Murray and Ellifritt (2001), Hancock (2003), Schafer (2002)). The short half-wavelength local buckling mode has been well researched and an effective width model developed by Von Karman et al (1932) to produce a simple model of the post-buckling reserve strength. The long half-wavelength flexural-torsional mode has been well researched by Timoshenko (1945), Vlasov (1961) and Trahair (1993) and was shown to have very little postbuckling reserve of strength. The intermediate half-wavelength distortional buckling mode has been researched at the University of Sydney in recent years by Hancock (1985), Lau and Hancock (1990), Kwon and Hancock (1992) and Yang and Hancock (2004), at Johns Hopkins University by Schafer (2002) and the Technical University of Lisbon, Portugal by Camotim and Silvestre (2004). What has been known for some time is that the distortional mode has a postbuckling strength which is generally less than that of local buckling. However, the nature of this postbuckling reserve is not clearly understood, particularly what precipitates failure.

Several early papers recognized the mode now known as the distortional mode. Thomasson (1978) called it a torsional mode and tried to prevent it experimentally by placing straps across the flanges. Sridharan (1982) called it a local-torsional mode and analysed it theoretically using a finite strip post-buckling analysis and perturbation theory. Sridharan demonstrated that soon after buckling in the distortional mode, yielding occurs in the lip either at the tip or the flange junction depending on which way the flange and lip move (inward or outward respectively). He concluded that "one likely consequence of buckling of an edge stiffener in its own plane would be the onset of plastic yielding; and the yielding of a member which has been the main source of stiffness cannot but hasten the collapse of the structure". However, experimentation such as that of Yang and Hancock (2004) has shown experimentally this not to be the case with substantial postbuckling reserve in line with the early work of Kwon and Hancock (1992) even when the lip has yielded and developed local plastic mechanisms. A further complication raised by Yang and Hancock was the difference between the strength when the lips moved inward generally with a lower strength than when they moved outward. This was confirmed theoretically more recently by the Generalised Beam Theory (GBT) models of Silvestre and Camotim (2004) for fixed ended sections.

The main purpose of this paper is to investigate postbuckling in the distortional mode using the finite element program ABAQUS. The distortional mode cannot be completely isolated from the local mode and so the interaction of local and distortional buckling is considered in the paper. The work of Von Karman et al. (1932) showed that the postbuckling behaviour could be explained by looking at the longitudinal stress redistribution around the section in the postbuckling range of behaviour. The same approach is used in this paper. In addition, strength design curves for distortional buckling of channels in compression are further validated against the ABAQUS models.

## 2 SECTIONS INVESTIGATED

The experimental research of Lau and Hancock included simple lipped channels down to 1.67 mm thickness and 450 MPa yield stress, the work of Kwon and Hancock included lipped

channels with intermediate stiffeners in the web down to 1.0 mm thickness and 500 MPa yield, and that of Yang and Hancock included lipped channels down to 0.42 mm thickness and 550 MPa yield stress. Intermediate stiffeners are used in the thinner material sections to raise the local buckling stress to be comparable with the distortional buckling stress for the thinner material. The problem with the intermediate stiffeners is that they make it difficult to understand the local and distortional postbuckling stress redistribution in the sections. It was therefore decided to investigate simple lipped channel sections in the 1 mm to 6 mm thickness range to better understand the postbuckling stress distributions which occur as a result of local, distortional and interaction buckling. Different yield stress values were used including very high values which allowed the postbuckled deformations to develop.

The basic section chosen was a simple lipped channel with an 80 mm web and 60 mm flange. The lip size was varied from 5 mm to 9 mm and the thickness from 1 mm to 6 mm. The reference graphs of buckling stress versus buckled half-wavelength from a semi-analytical finite strip buckling analysis (SAFSM) (Papangelis and Hancock, 1995), shown as a solid line, with ends simply supported but free to warp are shown for the 1 mm thick section with 5 mm lip in Fig. 1. The effect of fixing the ends as in a test is to increase the distortional buckling stress much more significantly than the local buckling stress. The results of a spline finite strip analysis (SFSM) (Lau and Hancock, 1986) between fixed ends are also shown as a solid line with circles in Fig. 1. It can be seen from Fig. 1 that the column with a lip size of 5 mm has a distortional buckling mode at approximately 300 mm buckle half-wavelength and buckling stress of 90 MPa. With the fixed ended condition of the spline finite strip analysis, the distortional buckling stress was increased to approximately 140 MPa, similar to the local buckling stress. This would allow for possible interaction of local and distortional buckling modes.

A 2 mm thick column with a lip size of 9 mm can be seen in Fig. 2 to exhibit a distortional buckling mode at approximately 300 mm buckle half-wavelength. Similar behaviour to that of the 1 mm thick section with 5 mm lip can be observed for the 2 mm thick section in Fig. 2. On the basis of these studies for a range of thicknesses and lip sizes, it was decided to study 6 mm, 3 mm and 2 mm thick sections with a 9 mm lip, and 2 mm and 1 mm thick sections with a 5 mm lip. These dimensions were chosen to produce pure distortional buckling in some cases (i.e. 6 mm thick section) and interaction buckling in some cases (i.e. 2 mm with 9 mm lip, 1 mm with 5 mm lip).

## 3 FINITE ELEMENT ANALYSIS

### 3.1 General

The finite element program ABAQUS (2004) version 6.4 was used to simulate the buckling behaviour of fixed-ended simple lipped channels. When analysing elastic deformations, the material is assumed to have a linear response and hence no plasticity is included. For the inelastic analysis, plastic strains are included. However since no actual experiments were carried out to determine the plastic strain data, the data was based on the Yang and Hancock (2002, 2006) stress-strain curves of G550 coupons in tension.

The simulation consists of two steps. In the first step, an elastic buckling analysis, also known as a linear perturbation analysis, was performed on a perfect column to obtain its buckling mode (eigenmode). This indicates the possible buckling mode of the structure. In the second step, a non-linear analysis was carried out on the model using the modified Riks method. Material plasticity strains and geometric imperfection, obtained from the previous

step, are included in this analysis so as to obtain the ultimate failure loads and failure modes of the columns.

### 3.2 Type of element and finite element mesh

ABAQUS includes general-purpose shell elements that provide robust and accurate solutions to most applications. Some of these general-purpose shell element types are the S3, S3R, S4 and S4R. Element type S4R is a four-node doubly curved general-purpose shell, reduced integration with hourglass control, using six degrees of freedom per node (ABAQUS, 2004) and was chosen to be used for the simulations.

Simpson's rule was chosen, by default, to calculate the cross-sectional behaviour of a shell. The shell element chosen, assuming a homogenous section, has five integration points through the thickness (ABAQUS, 2004). During the analysis, ABAQUS evaluates the stress and strain components on the top (positive) and bottom (negative) surfaces. For this research, in order to understand how the stresses are redistributed even through the element thickness, the stress and strain components are evaluated at the shell's top and bottom surfaces as well as at the midsurface.

The size of the finite element mesh used in the analysis is 5 mm x 5 mm (length by width) and was applied to both the webs and flanges. The lips have mesh sizes ranging from 5 mm x 2.5 mm to 5 mm x 4.5 mm. A typical finite element mesh of a buckled simple lipped channel is shown in Fig. 3.

### 3.3 Boundary conditions and method of loading

The simple lipped channel column was assumed to be compressed between fixed ends. This is done so by restraining the translational and rotational degrees of freedom at both ends of the model, except the translational degree of freedom in the axial direction at the top of the model. This allows for the compression due to the load application at the top end. All nodes other than at the ends are free to translate and rotate in any direction.

When analysing the local buckling component alone at the distortional length, the distortional buckling component has to be "locked out". This was achieved by restraining the lateral displacement of the nodes at the lip flange junction. This effectively "locked out" the distortional buckling mode so as to facilitate the analysis of the post-local buckling stress distribution.

The displacement control method was employed to simulate an applied load on the top end of the channel column. The applied compressive load was simulated by specifying an axial displacement of 2 mm at the top end of the column. This displacement is equivalent to the axial shortening of the column.

### 3.4 Material properties and material orientation

As mentioned earlier, a linear perturbation analysis is carried out to analyse the elastic buckling behaviour of the column and to provide the possible buckling modes (eigenmodes) of the column. In the linear analysis, only the density, Young's modulus and Poisson's ratio were included. In some of the analyses, the columns were analysed as having ideal elastic material behaviour, hence material plasticity was not included. However some analyses

allowed inelasticity and hence material plasticity values were added into the finite element models by specifying the “true” values of stresses and strains.

If the nominal data for a uniaxial test is obtained and the material is isotropic, the true stress ( $\sigma_{true}$ ) and true plastic strain ( $\varepsilon_{true}^{pl}$ ) can be simply converted by the following equations:

$$\sigma_{true} = \sigma(1 + \varepsilon) \quad (1)$$

$$\varepsilon_{true}^{pl} = \ln(1 + \varepsilon) - \frac{\sigma_{true}}{E} \quad (2)$$

where  $E$  is the Young’s modulus,  $\sigma$  and  $\varepsilon$  are nominal stress and strain respectively (ABAQUS, 2004). The measured stress and strain values were obtained from tensile coupon tests conducted by Yang and Hancock (2002, 2006). The yield stress used in this paper was assumed to be 700 MPa and the stress-strain curves are for the 0.42 mm material in Table 1 of that paper.

In order to determine the longitudinal stress distributions in the postbuckling range, the material has to be orientated into the longitudinal direction. This is done by assigning the material with a local coordinate system by using the \*ORIENTATION option in ABAQUS. During the orientation, each element is assigned to have the member 2-axis of the coordinate system in the axial direction.

### 3.5 Geometric imperfections

In the non-linear analysis, geometric imperfections are added onto the “perfect” model to create out-of-plane deformations. The geometric imperfections can be defined by three different methods in ABAQUS (ABAQUS, 2004). Firstly, the geometric imperfections can be defined by the linear superimposition of buckling modes. Secondly, they can be defined by the displacements from an initial \*STATIC analysis, which may consist of the application of a “dead” load. Thirdly, the imperfections can be defined by specifying specific nodes and modifying the translational degrees of freedom. In this report, the first method employing the linear superimposition of buckling modes was used.

Firstly, an initial analysis is carried out on a perfect mesh using the elastic buckling analysis to generate the possible buckling modes and, at the same time, nodal displacements of these modes are generated. Following this, the imperfection is introduced to the perfect mesh by means of linearly superimposing the elastic distortional buckling modes onto the mesh. However when analysing the elastic local buckling component at the distortional buckle half-wavelength, the local buckling mode is linearly superimposed onto the mesh. The lowest buckling modes are usually the critical modes, hence these are used to generate the imperfections. A scaling factor with respect to the thickness was applied to the imperfection before superimposing to create the perturbed mesh. To validate the analyses and investigate imperfection magnitudes, sensitivity and validation analyses were performed with different levels of geometric imperfections.

### 3.6 Analyses

#### 3.6.1 Eigenvalue buckling analysis

The eigenvalue buckling analysis is carried out to determine the buckling modes and to estimate the critical buckling stress of “stiff” structures. Stiff structures have very little deformation prior to buckling and primarily carry loads axially. When the response of a structure is non-linear before collapse, a general eigenvalue buckling analysis can provide useful estimates of collapse mode shapes (ABAQUS, 2004).

ABAQUS uses the subspace iteration eigensolver when the \*BUCKLE analysis is carried out. Eigenvalues, also known as load multipliers, are extracted in this analysis and the lowest value is most important. The buckling mode shapes, also known as eigenvectors, are often the most useful outcome in the eigenvalue analysis, since they predict the likely failure mode of the structure.

### 3.6.2 Postbuckling analysis

A structure that has material and geometrically nonlinearity or has unstable postbuckling response requires a load-displacement analysis to be performed. This analysis is known as the “modified Riks method” and is generally used to predict unstable, geometrically nonlinear collapse of a structure. The Riks method employs proportional loading and solves simultaneously for loads and displacements. ABAQUS uses the arc length along the static equilibrium path in load-displacement space to measure the progress of the solution. This method is useful as it provides solutions regardless of whether the response is stable or unstable.

The Riks method works well in snap-through problems – those in which the equilibrium path in load-displacement space is smooth and does not branch. The method can also be used to perform postbuckling analyses of structures exhibit stable and unstable postbuckling behaviours (ABAQUS, 2004). In order to analyse postbuckling behaviour, the model has to have a continuous response instead of bifurcation, and this is done so by adding the geometric imperfection to create a perturbed mesh. This allows for some response in the buckling mode before the critical load is reached.

## 4 SENSITIVITY AND VALIDATION ANALYSES

As part of this investigation, both outwards (O-O) and inwards (I-I) imperfections have been assumed where outwards refers to the lip motion relative to the other lip. Schafer and Pekoz (1998) recommended that for a distortional geometric imperfection (called Type 2), a value approximately equal to the plate thickness,  $t$ , can be chosen. However this value may be too large when applied as the maximum amplitude of a distortional buckling half-wave since it may produce conservative results for distortional buckling modes with increasing material thickness. A value of  $0.64t$  was obtained by Schafer and Pekoz from the lower bound probability of 25 % of the Type 2 imperfections and this value has been used to analyse and compare the FEA ultimate failure loads to known strength curves in Fig. 4. The curves are a strength curve ( $P_{uw}$ ) based on the Winter (1968) effective width formula and the Kwon and Hancock (1992) strength equation ( $P_{ukh}$ ), which is the same as used in the Direct Strength Method (DSM) in AS/NZS 4600:2005 (2005) and NAS (supplement) (2004). The elastic buckling curve ( $P_{od}$  or  $P_{ol}$ ) is shown as the solid line, while the Winter strength curve, for local buckling, is shown as the line with triangles (▲) and the Kwon and Hancock strength curve, for distortional buckling, as a line with circles (●). The Winter strength curve is derived from the Winter (1968) effective width as shown in Equations 3 and 4.

$$\frac{b_e}{b} = 1 \quad \lambda_l \leq 0.673 \quad (3)$$

$$\frac{b_e}{b} = \sqrt{\frac{f_{ol}}{f_y}} \left( 1 - 0.22 \sqrt{\frac{f_{ol}}{f_y}} \right) \quad \lambda_l > 0.673 \quad (4)$$

where,

$$\lambda_l = \sqrt{\frac{f_y}{f_{ol}}}$$

where,  $f_y$  is the yield stress and  $f_{ol}$  is the local buckling stress

When the effective width,  $b_e$ , of each element of a section is computed for each element in the section assuming that all buckle locally at the same stress  $f_{ol}$ , then multiplying by the plate thickness,  $t$ , and yield stress,  $f_y$ , and summing over all elements in the section produces

$$P_{uw} = P_y \quad \lambda_l \leq 0.673 \quad (5)$$

$$P_{uw} = \sqrt{\frac{P_{ol}}{P_y}} \left( 1 - 0.22 \sqrt{\frac{P_{ol}}{P_y}} \right) P_y \quad \lambda_l > 0.673 \quad (6)$$

where,

$$\lambda_l = \sqrt{\frac{P_y}{P_{ol}}}$$

where,  $P_y = Af_y$  and  $P_{ol} = Af_{ol}$

Equations 5 and 6 are called the Winter strength equations in this paper and apply to local buckling.

Equations 7 and 8 are the Kwon and Hancock strength equations and are similar to Equations 5 and 6 except that the coefficient 0.22 and the exponent 0.5 have been changed to 0.25 and 0.22 respectively lower the curve below the Winter strength equations and  $P_{ol}$  has been replaced by the distortional buckling load  $P_{od} = Af_{od}$ .

$$P_{ukh} = P_y \quad \lambda_d \leq 0.561 \quad (7)$$

$$P_{ukh} = \left[ 1 - 0.25 \left( \frac{P_{od}}{P_y} \right)^{0.6} \right] \left( \frac{P_{od}}{P_y} \right)^{0.6} P_y \quad \lambda_d > 0.561 \quad (8)$$

where,  $\lambda_d = \sqrt{\frac{P_y}{P_{od}}}$

Silvestre and Camotim (2004) also investigated the local and distortional postbuckling behaviour of lipped channel columns using Generalised Beam Theory (GBT) and finite element analyses. In their paper, the geometric imperfections were assumed to have an amplitude of  $0.15t$  which was applied to the finite element models for both the local and distortional buckling mode analyses. The FEA ultimate failure loads based on an

imperfection of  $0.15t$  are compared with the strength curves in Fig. 5 and are higher than those in Fig. 4 based on the  $0.64t$ . All values are summarised in Table 1.

It can be seen in Figs. 4 and 5 that at higher slenderness (i.e. the 1 mm thick section), the FEA results for columns with both imperfection magnitudes are slightly lower than the Kwon and Hancock strength curve. When the columns with 9 mm lips are analysed at a thickness of 2 mm, it can be seen from Figs. 4 and 5 that the ultimate loads are significantly lower compared to the Kwon and Hancock strength curve for both imperfection magnitudes. With thickness increasing to 3 mm and 6 mm, it can be seen from Fig. 4 that the analyses with an imperfection magnitude of  $0.64t$  produced much lower ultimate loads when compared to the strength curves, whereas analyses with an imperfection magnitude of  $0.15t$  produced ultimate loads that are well predicted by the strength curves as seen in Fig. 5. Some of these differences are due to the imperfection magnitudes which could include the roundedness of the stress-strain curve stockier sections.

The results of the sensitivity analyses based on the different geometric imperfection magnitudes are also summarised in Table 1. The difference in ultimate loads between the analyses with different imperfection magnitudes is approximately 1 % at a thickness of 1 mm. The difference in ultimate loads between the analyses with different imperfection magnitudes increases up to 12 % at a thickness of 2 mm with 9 mm lips. An additional analysis was carried out on a section with 2 mm thickness and with a lip size 5 mm and the ultimate loads are well predicted by the strength curves and have a difference of approximately 1 % between the analyses with different imperfection magnitudes. The differences in ultimate loads between the analyses with different imperfection magnitudes are approximately 3.6 % to 8.8 % for sections with thicknesses 3 mm and 6 mm respectively.

The sensitivity analysis confirms the initial statement that thinner materials (1 mm or less) is less sensitive to imperfection magnitudes as the difference in ultimate loads are relatively similar. However with thicker materials, the ultimate loads are sensitive to imperfections and with a larger imperfection, the FEA ultimate loads becomes lower when compared to the strength curves. The results of the analyses based on the geometric imperfection magnitude of  $0.15t$  are summarised in Table 1. Generally the scale factor of 15 % of the plate thickness provides ultimate loads which compare well with the strength curves which are based on tests. Therefore, the scale factor of 15 % of the plate thickness is chosen as the maximum amplitude of the geometric imperfections in the distortional mode to be applied to the finite element models for the later analyses in this paper. This choice is particularly important in this paper because thicker sections have been chosen in many of the analyses to separate the local and distortional modes.

To compare the FEA analyses with the Winter strength curve for local buckling, a set of additional analyses where distortional buckling was prevented was performed. The results of these analyses are summarised in Table 2. From Fig. 5, it can be seen that the local buckling strength, shown as a plus (+) symbol, for the sections with varying thicknesses are well predicted by the Winter strength curve based on a slenderness  $\lambda_l$  for local buckling of the whole section. For sections with thicknesses 1 mm and 2 mm, the FEA ultimate loads are slightly higher, whereas for the section at 3 mm thickness, the FEA ultimate load is slightly lower, which is most likely due to assumed imperfections.

## 5 POSTBUCKLING BEHAVIOUR

## 5.1 Load deflection curves

The ultimate loads from the postbuckling analyses with different thicknesses and distortional imperfection of maximum amplitude  $0.15t$  were discussed previously in Section 4. The load-deflection curves for the postbuckling analyses are shown in Figs. 6 to 10 for the sections with thicknesses 6 mm to 1 mm. In each figure, the inward and outward curves are plotted for a material that is assumed to remain elastic and with yielding also included. The inward and outward deflecting curves for the elastic material are defined as the square (■) and diamond (◆) lines respectively. Similarly the inward and outward deflecting curves for the material with yielding included are defined as the star (★) and cross (✖) lines respectively.

Comparing Figs. 6 to 10, it can be noted that as the sections get thinner, the elastic postbuckling curves become more separated with the inward curve always below the outward curve. This is due to the different stress redistributions across the section for the inward and outward deflection cases and will be further discussed in a later section. For the material with yielding included, the sections with thickness 6 mm, 3 mm and 2 mm with 9 mm lip failed below the critical distortional stress while sections with thickness 2 mm with 5 mm lip and 1 mm with 5 mm lip failed in the post-distortional stress range. For the sections that failed below the critical stress, it can be noted in Figs. 6 to 8 that the inward curve is higher than the outward curve at failure, but very quickly the curves cross over with the outward curve carrying more load after failure. It is interesting to note that this cross over point approaches the elastic curves as the material gets thinner. For the sections that failed in the post-distortional stress range, this cross over occurs in the elastic curve, hence it can be seen in Figs. 9 and 10 that outward curve is higher than the inward curve at failure. This shows that in the post-distortional buckling mode, the outward deflecting sections are stiffer than the inward deflecting sections. This confirms the results from Yang and Hancock (2004) that the outward deflecting sections are stiffer than the inward deflecting sections for thin materials. For thin materials (e.g. 1 mm), it can be seen in Fig. 10 that for loads up to approximately 90 % of the failure load, which is approximately  $1.3 P_{crd}$ , there is not much difference between the elastic and inelastic behaviour of the section. Hence this section is useful to demonstrate how distortional buckling interacts with local buckling. This will be further discussed in a later section when the stress redistribution across the section is analysed.

## 5.2 Longitudinal stress distributions

The main objective of this report is to investigate the post-distortional stress distribution and the effects of post-local buckling on post-distortional buckling behaviour. The method of looking at the longitudinal stress distribution over a section is similar to that of Von Karman et al (1932). Longitudinal stress distributions are given for sections with thicknesses 6 mm in Figs. 11 to 16, 3 mm in Figs. 17 to 22 and 1 mm in Figs. 23 to 28. The 6 mm section demonstrates a section undergoing post-distortional stress redistribution while at the other extreme, the section with 1 mm thickness demonstrates the effects of distortional buckling on the post-local buckling stresses. In this report, the stress distributions are provided for the inward and outward deflection cases when the material remains elastic and with yielding included. In addition, the local buckling stress distribution at the distortional length is also investigated.

### 5.2.1 Section with 6 mm thickness

The longitudinal stress distributions for the section with inward (I-I) and outward (O-O) deflections when the material is assumed to remain elastic is shown in Figs. 11 and 12

respectively. The analysis of the section with this thickness was chosen because it had an elastic distortional buckling stress ( $F_{\text{crd}} = 2132 \text{ MPa}$ ) much less than the elastic local buckling stress ( $F_{\text{crl}} = 5347 \text{ MPa}$ ). The ratio of  $F_{\text{crl}}$  to  $F_{\text{crd}}$  is approximately 2.51 as given in Table 2. For both cases, the sections deformed in the post-distortional mode since the stresses were well below those where local buckling effects might have affected it.

When the stresses are redistributed across the web in the post-distortional buckling region, the stresses decrease in the middle as it sheds the stresses to the flange-web junctions. However for the inward and outward deflections, the increased stresses at the junctions are different at similar load levels. When  $P/P_{\text{crd}}$  is approximately 1.35, the stress at the flange-web junction is approximately 3890 MPa for the inward deflection mode, while the stress at the flange-web junction for the outward deflection mode is approximately 4350 MPa. Thus it can be noted that in the post-distortional range, the flange-web junction of the outward mode carries more load than the inward mode at the same load level for a section with thickness 6 mm. This increased stress capacity for the section with outward deflection mode compared to the inward deflection mode indicates that the inward deflection mode is much softer as it sheds the load more rapidly as the deformations progress, as shown in Fig. 13. This confirms the results obtained by Yang and Hancock (2004) that the outward deflection modes are stiffer than the inward deflection modes.

When the distortional mode was “locked out” so as to observe the local buckling stress alone at the distortional length, the stress distribution for the post-local buckling range for the section is as shown in Fig. 14. It can be seen that as the load increases, there is significant stress redistribution in the middle of the web and flanges to the flange-web and flange-lip junctions as for normal post-local buckling behaviour. Figs. 11 and 12 also show that as the loads increase into the post-distortional buckling region, the stresses in the middle of the web and flanges are redistributed to the flange-web and flange-lip junctions. However, it is interesting to note that this post-distortional buckling stress redistribution has a unique characteristic which has some similarities to the post-local buckling stress distribution shown in Fig. 14, particularly for the inward deflection mode shown in Fig. 11.

The longitudinal stress distributions for the section with inward and outward deflection cases now including yielding is shown in Figs. 15 and 16 respectively. For the section with inward deflection, the stress at the web and flanges are redistributed to the flange-web and flange-lip junctions relatively equally and hence yield approximately at the same time. The stress in the web and flanges for the section with the outward deflection are redistributed differently with most of the stress being shed to the lips and flange-web junctions. Due to the stress concentrating at the junction, the section fails at a slightly lower load when compared to the inward mode, with the lips yielding first but failure occurring in the junctions.

### 5.2.2 Section with 3 mm thickness

The longitudinal stress distributions for the 3 mm thick section with inward and outward deflections when the material is assumed to remain elastic is shown in Figs. 17 and 18 respectively. The analysis of the section with this thickness was chosen because the section failure loads were in the region of the elastic local buckling stress. The elastic distortional buckling stress ( $F_{\text{crd}}$ ) and elastic local buckling stress ( $F_{\text{crl}}$ ) are 821 MPa and 1420 MPa respectively and the ratio of  $F_{\text{crl}}$  to  $F_{\text{crd}}$  is approximately 1.73 as given in Table 2. When  $P/P_{\text{crd}}$  is approximately 1.33, the stress at the flange-web junction is approximately 1700 MPa for the inward deflection mode as shown in Fig. 17, while the stress at the flange-web junction for the outward deflection mode is approximately 1800 MPa as shown in Fig. 18.

Hence it is similar to the previous analysis with thickness 6 mm where the flange-web junction of the outward deflection mode carries more load than the inward deflection mode.

Similar to the previous analysis, the flange-web junction of the outward deflection mode carries more load than the inward deflection mode as the inward deflection mode is softer as shown in Fig. 19. This confirms the results obtained by Yang and Hancock (2004) that the outward deflection modes are stiffer than the inward deflection modes. This causes the section with inward deflection to redistribute the stress in the web to the flange-web and flange-lip junctions more rapidly.

When the distortional mode was “locked out” so as to observe the local buckling stress at the distortional length, the stress distribution for the post-local buckling range for the section is as shown in Fig. 20. The post-distortional buckling stress distribution for the inward deflection mode (Fig. 17) has a similar characteristic to the post-local buckling stress distribution as previously observed with thickness 6 mm. As the load increases, the stress in the web decreases in the middle and is rapidly shed to the flange-web junctions. When the load applied was approximately  $0.8 P_{cr1}$ , which is equivalent to approximately  $1.39 P_{crd}$ , the stress at the flange-web junction is approximately 1300 MPa as shown in Fig. 20. The post-local buckling stress at load level  $1.39 P_{crd}$  can be compared to the stress at the flange-web junction at the load  $1.33 P_{crd}$  (1700 MPa) of the section with inward deflection mode (Fig. 17). This comparison shows that the effect of the distortional buckling on the post-local buckling stress is to push the stress higher at the flange-web junction, causing the section to fail at the flange-web junction with a higher stress concentration. Therefore this demonstrates the effect of interaction of local and distortional buckling in the postbuckling range is to increase stresses at the flange-web junctions.

The longitudinal stress distributions for the section with inward and outward deflection cases with yielding are shown in Figs. 21 and 22 respectively. Even though the inward mode has less stiffness, the stresses in the web and flanges are redistributed relatively equally into the flange-web and flange-lip junctions, allowing the section to carry a higher load ( $0.688 P_{crd}$ ) with failure occurring at the flange-lip junctions as shown in Fig. 21. Compared to the outward mode, the stresses are distributed differently with the stresses concentrating at the lips and flange-web junctions. From Fig. 22, it can be seen that the lips yield first but the section continues to carry load until failure occurs at the flange-web junctions at load level  $0.665 P_{crd}$ . The failure load of the outward deflection mode is slightly lower than the inward deflection mode in this case.

### 5.2.3 Section with 1 mm thickness

The longitudinal stress distributions for the 1 mm thick section with inward and outward deflections when the material is assumed to remain elastic is shown in Figs. 23 and 24 respectively. The analysis of the section with this thickness was chosen because the elastic distortional buckling stress was approximately equal to the elastic local buckling stress. The elastic distortional buckling stress ( $F_{crd}$ ) and elastic local buckling stress ( $F_{cr1}$ ) are 154 MPa and 163 MPa respectively and the ratio of  $F_{cr1}$  to  $F_{crd}$  is approximately 1.06. When  $P/P_{crd}$  is approximately 1.3, the stress at the flange-web junction is approximately 420 MPa for the inward deflection mode (Fig. 23), while the stress at the flange-web junction for the outward deflection mode is approximately 400 MPa (Fig. 24). It is interesting to note that at this thickness, the stress at the flange-web junction for the inward deflection is now higher than the outward deflection.

The lip displacements of the deflection modes are shown in Fig. 25 and although, as mentioned earlier, the flange-web junction of the outward deflection mode carries slightly more load than the junction of the inward deflection mode, it can be seen that the inward deflection mode is softer than the outward deflection mode. This confirms the results obtained by Yang and Hancock (2004) that the outward deflection modes are stiffer than the inward deflection modes. With this increased stiffness, the outward mode fails at a higher load compared to the inward mode, as shown in the results in Fig. 5.

When the distortional mode was “locked out” so as to observe the local buckling stress at the distortional length, the stress distribution for the post-local buckling range for the section is as shown in Fig. 26. When the load applied was approximately  $1.28 P_{cr1}$ , which is equivalent to approximately  $1.36 P_{crd}$ , the stress at the flange-web junction is approximately 261 MPa as shown in Fig. 26. This post-local buckling stress of 261 MPa can be compared to the stress at the flange-web junction at  $1.3 P_{crd}$  (420 MPa) for the inward deflection mode (Fig. 23). This is similar to the analysis carried out earlier on thickness 3 mm, whereby the effect of the distortional buckling on the post-local buckling stress is to push the stress higher at the flange-web junction. This shows the interaction of local and distortional buckling in the postbuckling range, which can be described by comparing Figs. 23 and 26. In Fig. 26, as the load increases into the post-local buckling range,  $0.99 P_{cr1}$  to  $1.45 P_{cr1}$ , the stresses in the centre of the web decreases to approximately 70 MPa, while the stresses in the flanges increase to approximately 175 MPa. This increased stress at the middle of the flange causes less stress to be redistributed to the junctions. In Fig. 23, as the load increases into the post-distortional buckling range,  $1.0 P_{crd}$  to  $1.3 P_{crd}$ , the stress in the web decreases in a similar fashion to the post-local buckling behaviour. However the stresses in the flanges decrease very slightly and are redistributed into the junctions, causing the flange-web junctions to be more highly stressed.

The longitudinal stress distributions for the section with inward and outward deflection cases with yielding are shown in Figs. 27 and 28 respectively. The purpose of analysing both with and without yielding at this thickness was to observe whether the lip failure significantly influenced the behaviour. It can be observed for the inward deflection mode that up to 90 % of the failure load, which is approximately  $1.3 P_{crd}$  as seen in Fig. 10, there is not much difference between the elastic and inelastic behaviour around the section except maybe the stresses in the centre of the flanges as shown in Figs. 23 and 27. The maximum load still does not occur until the flange-web junction yielding occurs. Hence, although the lip yielding does cause some readjustment of the stresses, it is still the flange-web junction failure which governs the failure of the section and failure for the inward deflection mode occurs at a load of  $1.445 P_{crd}$ . By comparison with the inward deflection mode, the outward mode fails at the yielding of the lips even though this is a higher load ( $1.54 P_{crd}$ ) due to the different stress distributions as seen in Fig. 28.

### 5.2.3.1 Effect of lip yielding on failure load

In the previous section, it was discussed that a section with thickness 1 mm, lip yielding may occur but not cause failure of the section and that it is the flange-web junction that is normally the critical factor. Therefore to understand the effect of lip yielding on the failure load, a section (80mm x 60mm x 5mm, 1 mm thickness) similar to the previously analysed sections was designed with a new material, i.e. a different yield stress, that is applied to the lips. By increasing the yield stress to approximately 1700 MPa, the yielding of the lips will be prevented.

Fig. 29 compares the load displacement plots for the inward and outward deflection modes for the sections with both one and two materials. The section with one material is the previously analysed section in Section 5.2.3. Figs. 30 and 31 show the longitudinal stress distributions for the inward and outward deflection modes respectively for the sections with two materials. For the inward deflection mode, it can be seen from Fig. 30 that the failure load is approximately  $1.505 P_{crd}$  and this presents a 4.15 % increase from the failure load of  $1.445 P_{crd}$  as shown in Fig. 27 for the section with one material. This increase is considered to be not significant. For the outward deflection mode, it can be seen from Fig. 31 that the failure load is  $1.61 P_{crd}$  and this presents a 4.48 % increase from the failure load of  $1.54 P_{crd}$  as shown in Fig. 28 for the section with one material. This increase is considered to be not significant. Therefore it can be concluded that lip yielding does not play a large part in the section failure while failure occurs very soon after yielding at the flange-web junction. This is confirmed by Yang (2004) with the 800 mm column failing in the outward deflection mode where local failure occurred in the lips at about 18 kN but the section continued to carry load to approximately 22 kN with very little apparent effect.

## 6 TEST RESULTS IN RELATION TO STRENGTH DESIGN CURVES WITH 0.5 AND 0.6 COEFFICIENTS

With the analyses carried out, the distortional buckling results were compared to the strength design curves based on the Kwon and Hancock strength equation as given in Section 4. The validation of the Winter strength curve for local buckling was based on an additional set of analyses and was previously discussed in Section 4. The ratios of  $P_{cr1}$  to  $P_{crd}$  for the varying thicknesses are summarised in Table 2. From Table 2, it can be noted that when sections with a larger ratio of elastic local to distortional buckling stress, i.e. sections with thicknesses 6 mm, 3 mm and 2 mm (5 mm lip), the failure mode is purely distortional buckling and the results are generally well predicted by the Kwon and Hancock strength curve. These sections, without interaction of buckling modes, have strength results approximately -0.57 % to 2.6 % of the Kwon and Hancock strength curve. When the ratio of elastic local to distortional buckling stress is approximately 1.0, i.e. sections with thicknesses 2 mm (9 mm lip) and 1 mm (5 mm lip), interaction of local and distortional buckling would most likely occur and cause the test results to be lower than the Kwon and Hancock strength curve. When a section has interaction of buckling modes, the effect of this interaction causes the section to have a strength reduction of approximately 9.3 % to 10 % as previously summarised in Table 1.

Hence from the analyses of sections failing in the local and distortional modes, the Winter and Kwon and Hancock strength curves are appropriate to be used to predict sections failing purely in the local or distortional mode with no interaction of buckling modes. When interaction of buckling modes occurs, the strength of the section is reduced and the design strength curves are unable to account for this reduction.

## 7 CONCLUSION

This paper has described the finite element analysis and results of the postbuckling in the local and distortional modes of thin-walled section with edge stiffeners of varying thicknesses. The effect of the distortional buckling mode on the post buckling stress distributions was investigated and discussed. The column was designed with fixed-ended boundary conditions. The finite element program, ABAQUS, was used to create a finite

element model by using shell elements. In this finite element model, geometric imperfections, method of load application, material orientation and non-linearity were developed and discussed. A sensitivity analysis for the magnitude of geometric imperfections in the distortional mode of the columns was carried out and the results were compared to known strength curves to validate the methodology against tests.

Load deflection curves were generated for the sections with and without yielding, which included inward and outward distortional modes and the results were discussed. Further analysis on sections with thicknesses 6 mm, 3 mm and 1 mm was carried out to observe the longitudinal stress distributions over these sections in the post-distortional and post-local buckling range. This methodology of analysing the stress redistribution of the section was adopted from an earlier method by Von Karman et al (1932) to analyse the post-local buckling behaviour. The following conclusions were determined from the analyses of the stress redistributions of the sections undergoing mainly distortional buckling but with local buckling also in the thinner sections.

1. The post-distortional buckling stress distribution has a unique characteristic which has similarities to the post-local buckling stress distributions with a significant stress redistribution in the web, particularly for the inward distortional mode. This explains why post-distortional buckling is higher than post-flexural or flexural-torsional buckling.
2. When local and distortional buckling interact in the postbuckling range, the effect of distortional buckling on the post-local buckling stress is to push the stress higher at the flange-web junctions.
3. The inward and outward distortional modes have very different stress distributions. The inward mode redistributes stresses in the web and flanges into the flange-web and flange-lip junctions. The outward mode distributes stresses mainly to the flange-web junctions and lips.
4. Failure tends to occur very soon after yielding of the flange-web junctions and lip yielding does not play a large part in the failure as had been predicted in earlier papers.
5. With thicker materials (3 mm and 6 mm), at similar load levels, the outward deflection mode has higher stress at the flange-web junctions compared to the inward deflection modes. With the thinner material (1 mm) the flange-web junction of the inward deflection mode has a slightly higher stress value compared to the outward deflection mode.
6. The section has a higher axial stiffness for the outward mode compared to the section deforming mainly in the inward mode. For the section with thinner material, the analysis showed that the distortional mode deflecting outwards has a greater strength. This confirms Yang's (2004) tests that showed the differences in strength when deflecting inwards and outwards. This was also confirmed theoretically by the Generalised Beam Theory (GBT) models of Silvestre and Camotim (2004) for fixed ended sections.
7. The Winter strength curve is validated by the local buckling analyses, while the distortional buckling analyses showed that the Kwon and Hancock strength curve validates the FEA results with pure distortional failure modes. The interaction of

local and distortional buckling modes indicated that there would be a reduction in section strength when the local and distortional buckling stresses are approximately equal.

The conclusions of this paper afford a much better understanding of failure in the post-distortional mode. In particular, the reasons why channel sections have a post-distortional strength which is not as significant as post-local strength have been explained. Further research is required to quantify the reductions due to the interaction of local and distortional buckling modes now that the mechanism is understood.

## **ACKNOWLEDGEMENTS**

This report forms part of an ARC research project entitled “Interaction of local and distortional buckling modes in cold-formed high strength steel” being carried out at the School of Civil Engineering at the University of Sydney. The authors would like to thank the Australian Research Council for the financial support for the project performed at the University of Sydney.

## REFERENCES

- ABAQUS version 6.4; User's manual.* (2004), ABAQUS, Inc., Pawtucket, R.I.
- American Iron and Steel Institute (AISI), (2004), *Supplement 2004 to the North American Specification for the design of cold-formed steel structural members, 2001 edition*, Washington, D.C.
- Camotim, D., Silvestre, N., (2004), "GBT-based analysis of the distortional postbuckling behaviour of cold-formed steel Z-section columns and beams", *Proceedings of Fourth International Conference on Thin-Walled Structures* (Loughborough, 22-24/6), 2004, pp 243-250.
- Hancock, G.J., (1985), "Distortional buckling of steel storage rack columns", *Journal of Structural Engineering*, v111, n 12, Dec 1985, pp 2770-83.
- Hancock G.J., (2003), "Cold-formed steel structures", *Journal of Constructional Steel Research*, v59(4), April 2003, pp 473-487.
- Hancock G.J., Murray T.M. and Ellifritt D.S., (2001), *Cold-formed steel structures to the AISI Specification.*, Marcel Dekker, New York.
- Kwon Y.B. and Hancock G.J., (1992), "Tests of cold-formed channels with local and distortional buckling", *Journal of Structural Engineering*, v117, n7, pp 1786-1803.
- Lau, S.C.W. and Hancock, G.J., (1986), "Buckling of thin flat-walled structures by a spline finite strip method", *Thin-Walled Structures*, v 4, n 4, pp 269-94.
- Lau, S.C.W. and Hancock, G.J. (1990), "Inelastic buckling of channel columns in the distortional mode", *Thin-Walled Structures*, v 10, n 1, 1990, pp 59-84.
- Papangelis, J.P. and Hancock, G.J., (1995), "Computer analysis of thin-walled structural members", *Computers & Structures*, v 56, Issue 1, pp 157-76.
- Schafer B.W., Pekoz T., (1998), "Computational modelling of cold-formed steel: characterizing geometric imperfections and residual stresses". *Journal of Constructional Research*, v 47, pp 193-210.
- Schafer, B.W., (2002), "Local, distortional, and Euler buckling of thin-walled columns", *Journal of Structural Engineering*, v 128, n 3, March 2002, pp 289-299.
- Silvestre, N. and Camotim, D., (2004), "Local-plate and distortional post-buckling behaviour of cold-formed steel lipped channel columns with intermediate stiffeners", *Proceedings of Seventeen International Speciality Conference on Cold-Formed Steel Structures* (Orlando, 4-5/11), 2004, pp 1-18.
- Sridharan, S., (1982), "Semi-analytical method for the post-local-torsional buckling analysis of prismatic plate structures", *International Journal for Numerical Methods in Engineering*, v 18, n 11, Nov 1982, pp 1685-1697.

Standards Australia / Standards New Zealand (2005), *Cold-formed steel structures-AS/NZS 4600:2005*, Sydney, NSW, Australia.

Thomasson, P.O., (1978), "Thin-walled C-shaped panels in axial compression", *National Swedish Building Research, D1:1978*.

Timoshenko, S.P., (1945), "Theory of bending, torsion and buckling of thin-walled members of open cross section", *Journal of the Franklin Institute*, v 239, Issue 5, May 1945, pp 343-361.

Trahair, N. S., (1993), *Flexural-torsional buckling of structures*, First edition, E & F N Spon.

Vlasov, V. Z., (1961), *Thin-walled elastic beams*, Moscow (English translation Israel Program for Scientific Translation, Jerusalem).

Von Karman, T., Sechler, E.E. and Donnell, L.H., (1932), "The strength of thin plates in compression", *Transactions ASME*, v 54, MP 54-5.

Winter, G., (1968), "Thin-walled structures-Theoretical solutions and test results", *Preliminary Publications of the Eighth Congress, IABSE*, pp 101-112.

Yang, D. and Hancock, G.J., (2004), "Compression Tests of Cold-Reduced High Strength Steel Channel Columns Failing in the Interaction Between Local and Distortional Modes", *Journal of Structural Engineering*, v 130, n 12, pp 1954-1963.

Yang, D., (2004), *Compression Stability of High Strength Steel Sections with Low Strain-Hardening*, Ph.D. Thesis, School of Civil Engineering, University of Sydney, Sydney.

Yang, D. and Hancock, G.J., (2006), "Numerical simulation of high-strength steel box-shaped columns failing in the local and overall buckling modes", *Journal of Structural Engineering*, v 132, n 4, pp 541-549.

## NOTATIONS

$A_e$	Effective area ( $\text{mm}^2$ )
$b$	Width of element (mm)
$b_e$	Effective width of element (mm)
$E$	Young's modulus (GPa)
$F_{\text{crd}}$	Critical distortional buckling stress (MPa)
$F_{\text{crl}}$	Critical local buckling stress (MPa)
$F_y$	Yield stress (MPa)
$P_{\text{crd}}, P_{\text{od}}$	Critical distortional buckling load (kN)
$P_{\text{crl}}, P_{\text{ol}}$	Critical local buckling load (kN)
$P_y$	Squash load (kN)
$P_{\text{ukh}}$	Ultimate load for Kwon and Hancock strength curve (kN)
$P_{\text{uw}}$	Ultimate load for Winter strength curve (kN)
$t$	Thickness (mm)
$\sigma$	Nominal stress (MPa)
$\varepsilon$	Nominal strain (MPa)
$\sigma_{\text{true}}$	True stress (MPa)
$\varepsilon_{\text{true}}^{\text{pl}}$	True plastic strain (MPa)
$\lambda_{\text{d}}$	non-dimensional slenderness for distortional
$\lambda_{\text{l}}$	non-dimensional slenderness for local

# FIGURES

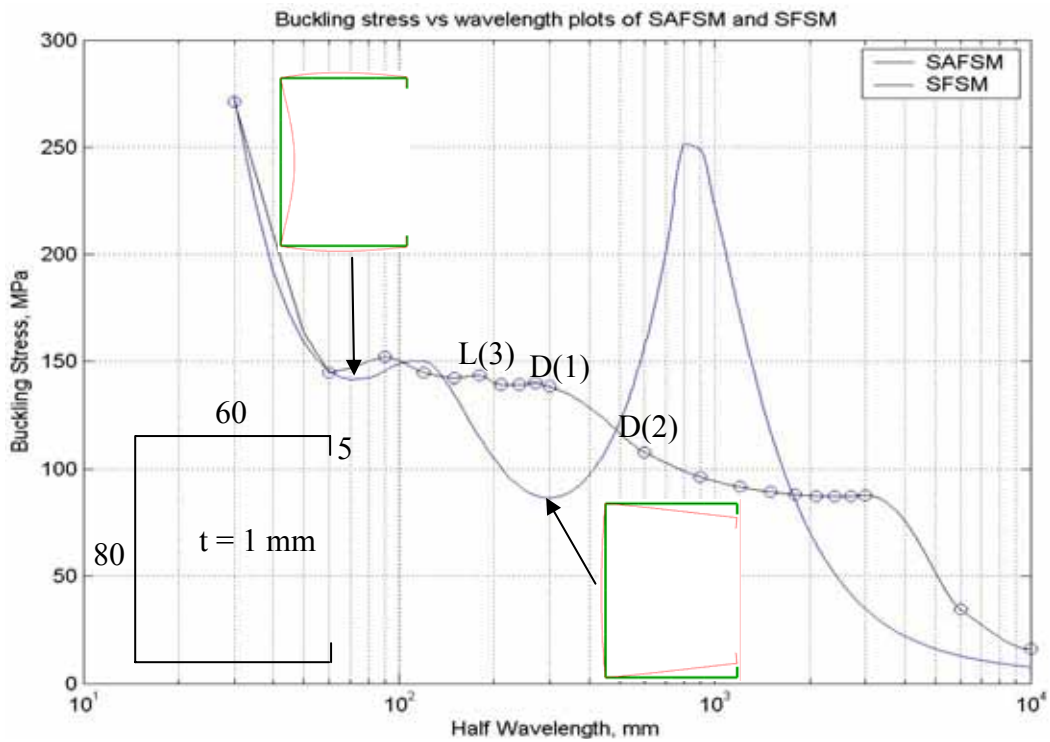


Figure 1 Plot of buckling stress vs buckle half-wavelength for 1 mm thick section with 5mm lip

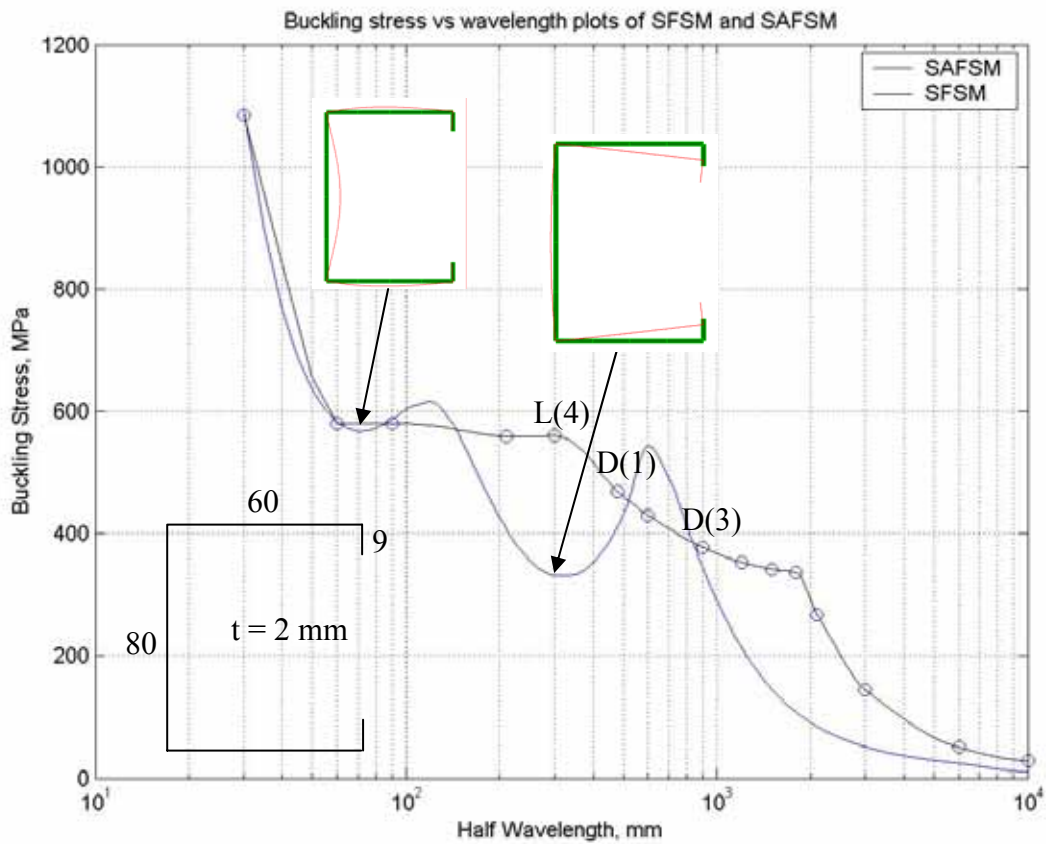


Figure 2 Plot of buckling stress vs buckle half-wavelength for 2 mm thick section with 9mm lip

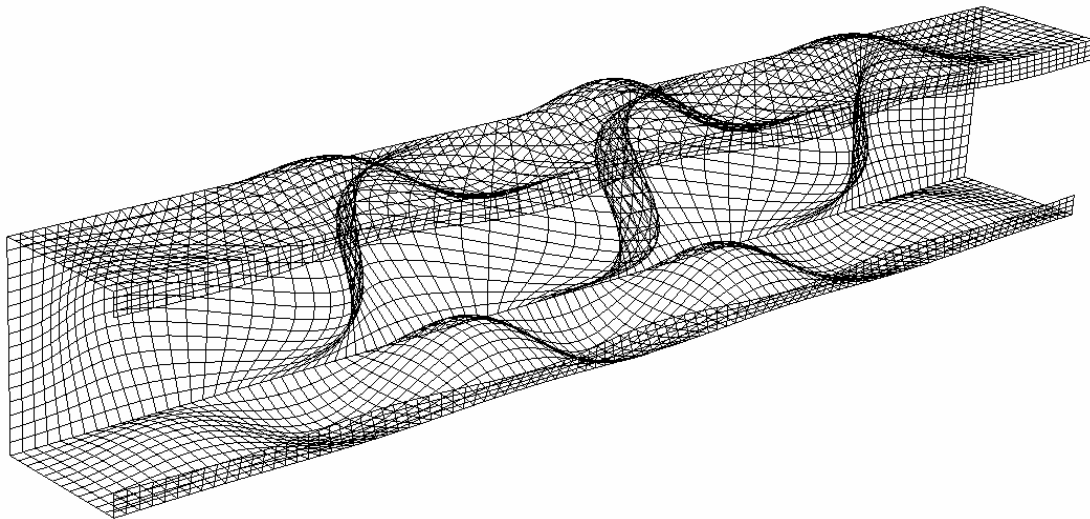


Figure 3 Finite element mesh of simple lipped channel

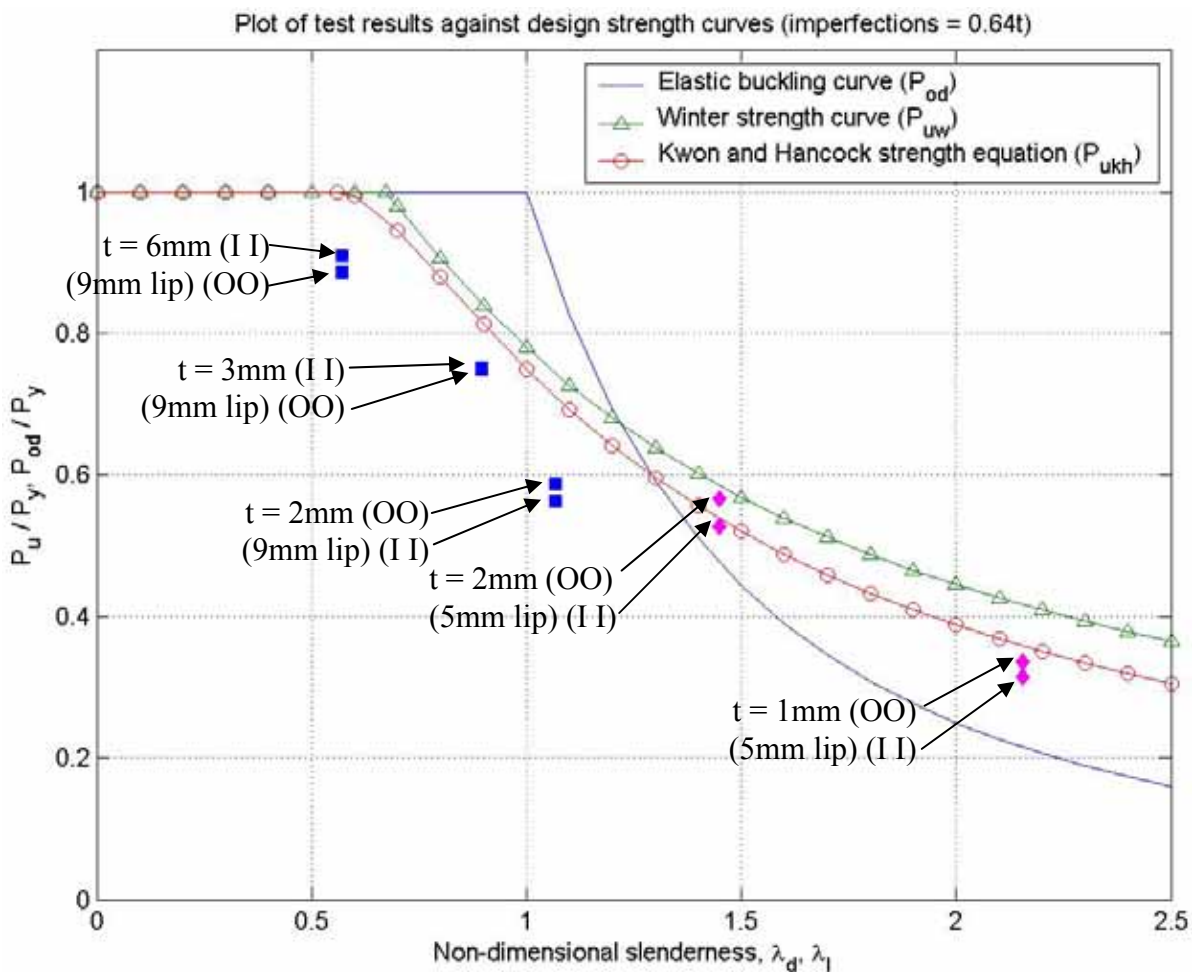


Figure 4 FEA results compared to strength curves with imperfections 0.64 t

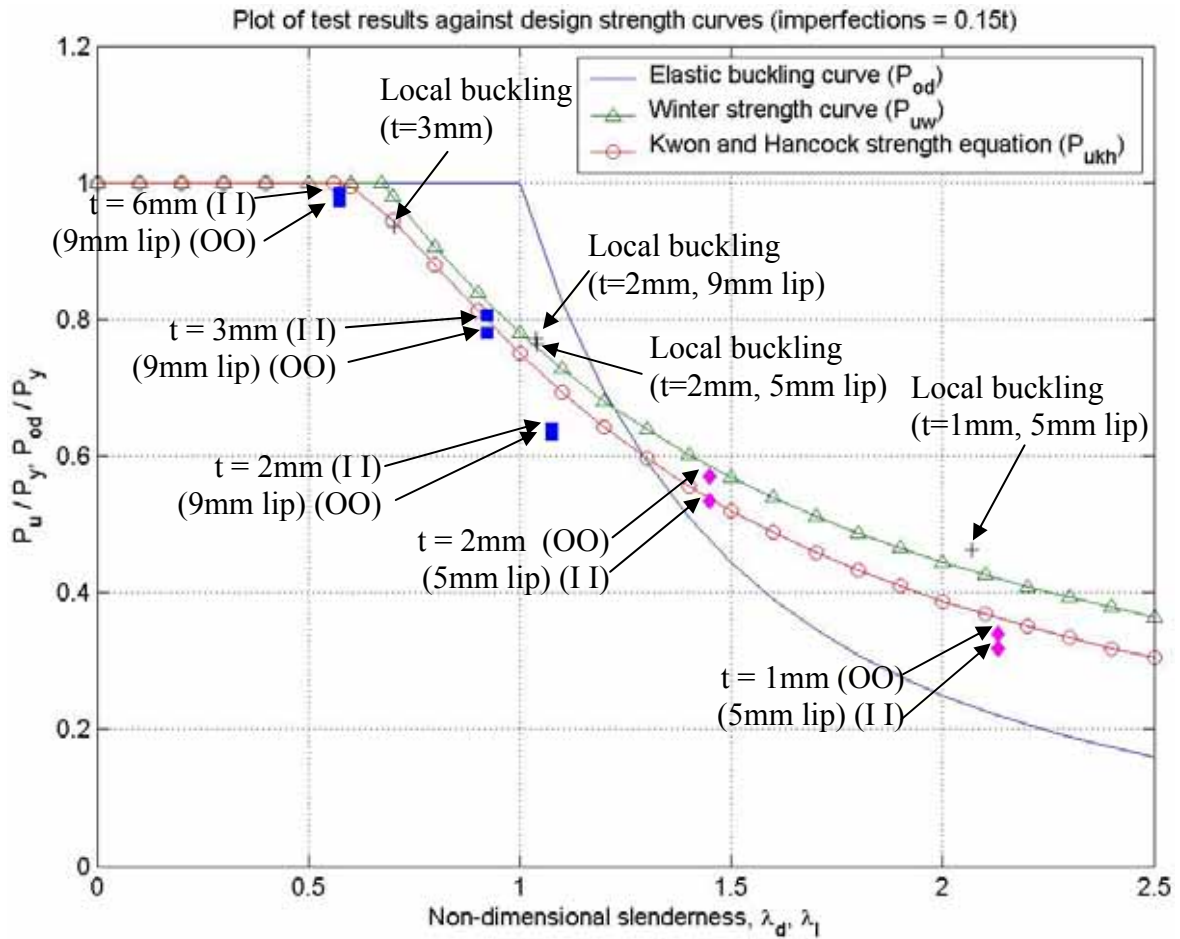


Figure 5 FEA results compared to strength curves with imperfections 0.15 t

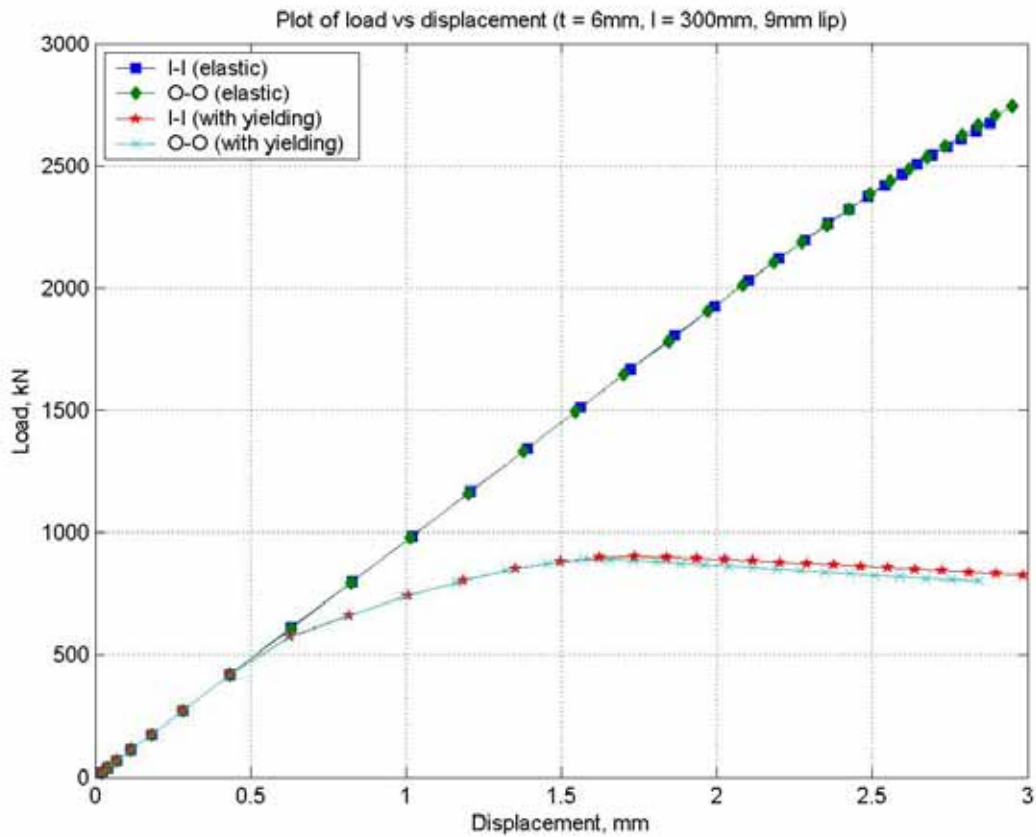


Figure 6 Plot of load vs axial shortening with  $t = 6\text{ mm}$  (9mm lip)

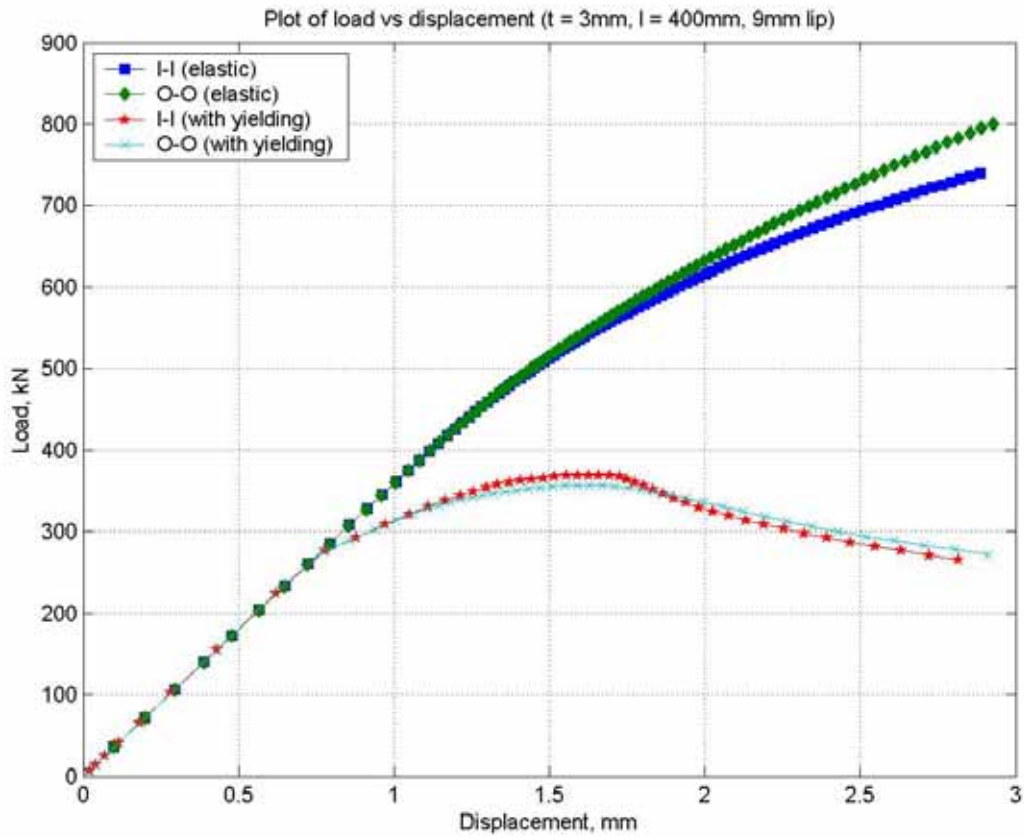


Figure 7 Plot of load vs axial shortening with  $t = 3\text{ mm}$  (9 mm lip)

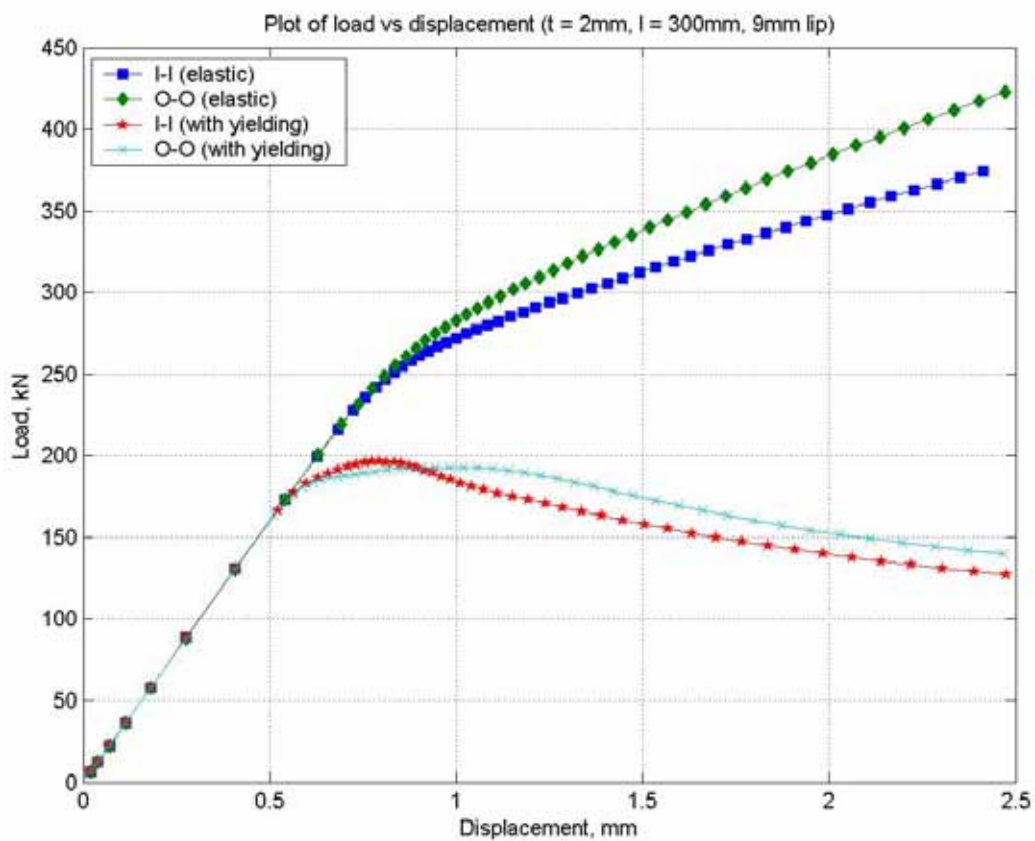


Figure 8 Plot of load vs axial shortening with  $t = 2\text{ mm}$  (9mm lip)

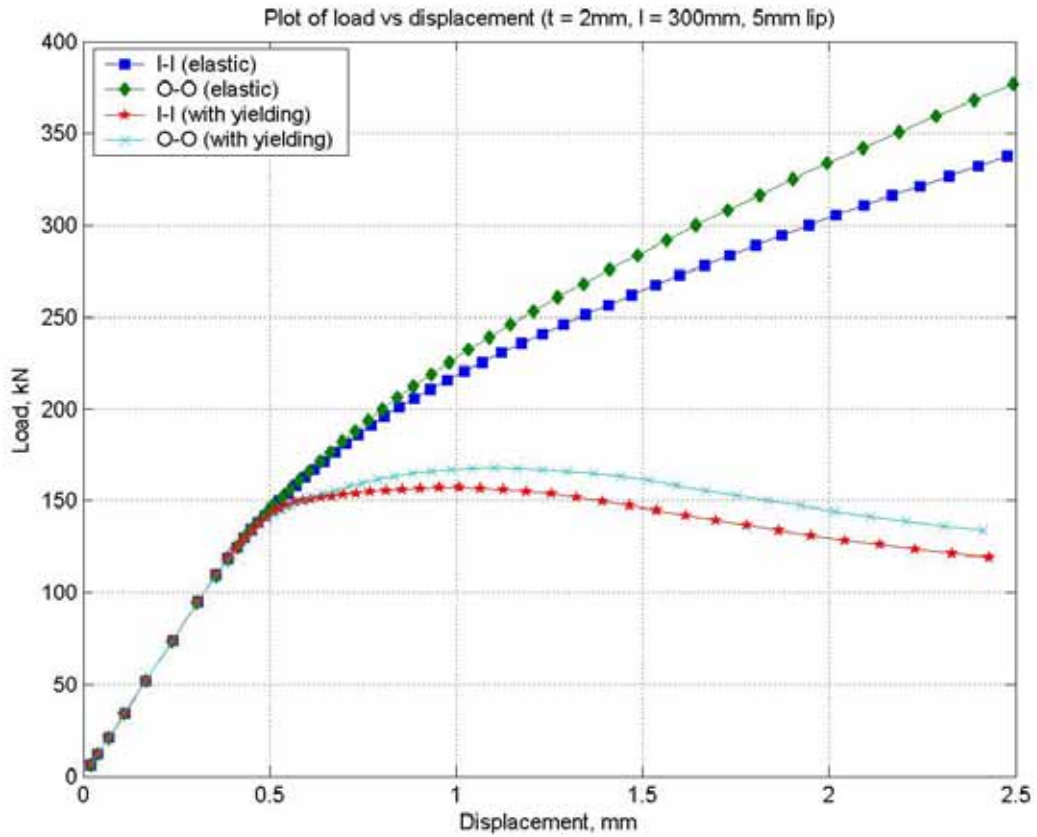


Figure 9 Plot of load vs axial shortening with  $t = 2\text{ mm}$  (5mm lip)

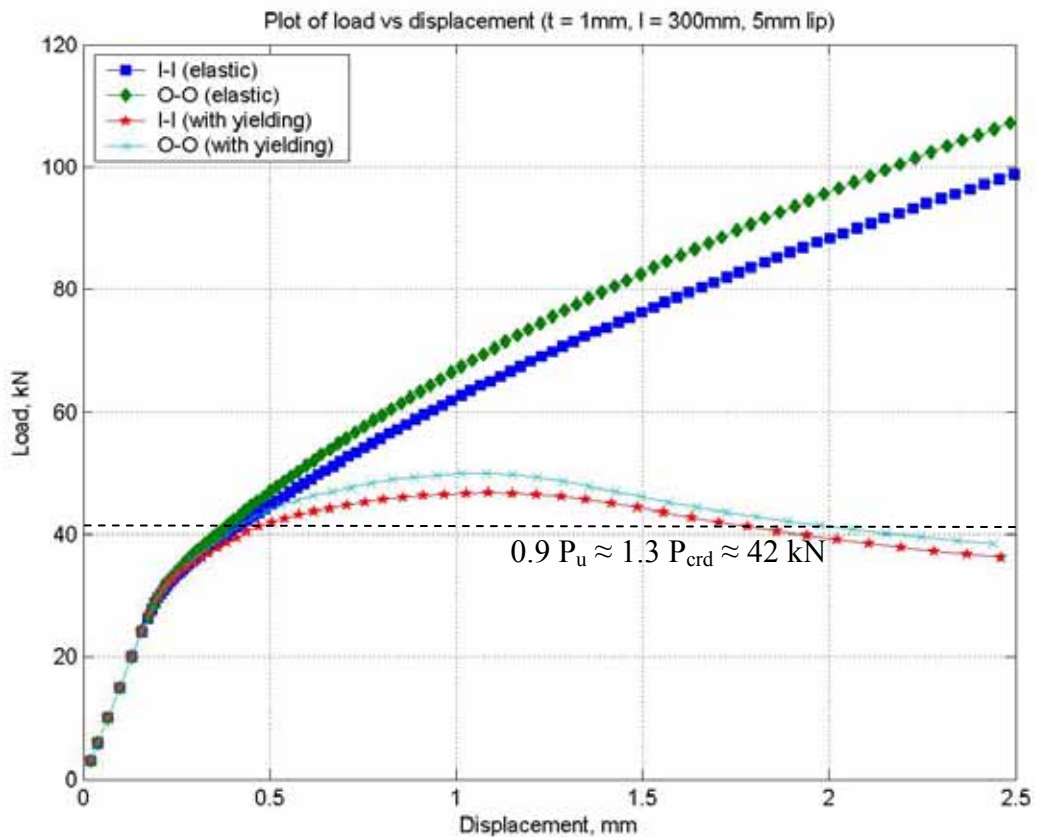


Figure 10 Plot of load vs axial shortening with  $t = 1\text{ mm}$  (5mm lip)

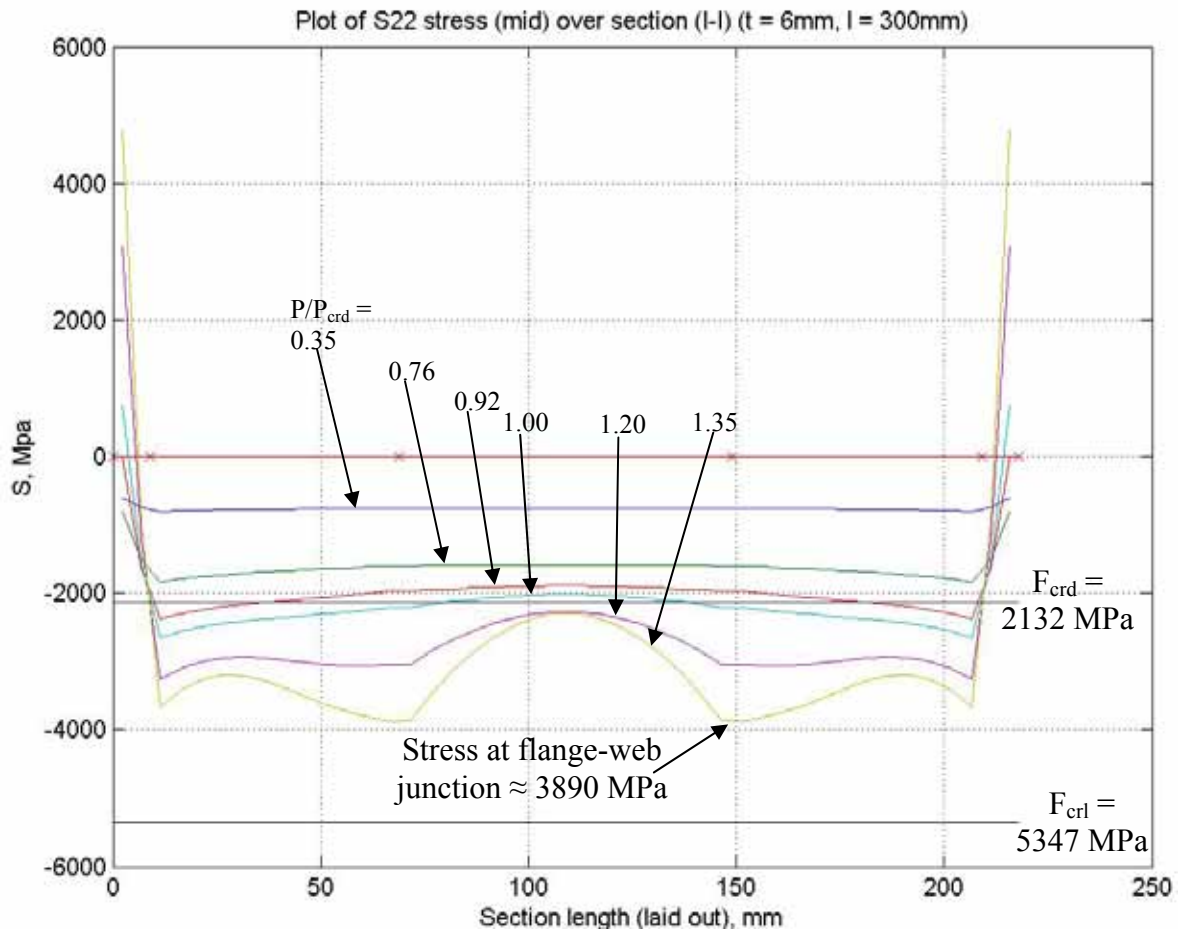


Figure 11 Plot of longitudinal stress distribution around section for t=6mm (I-I)

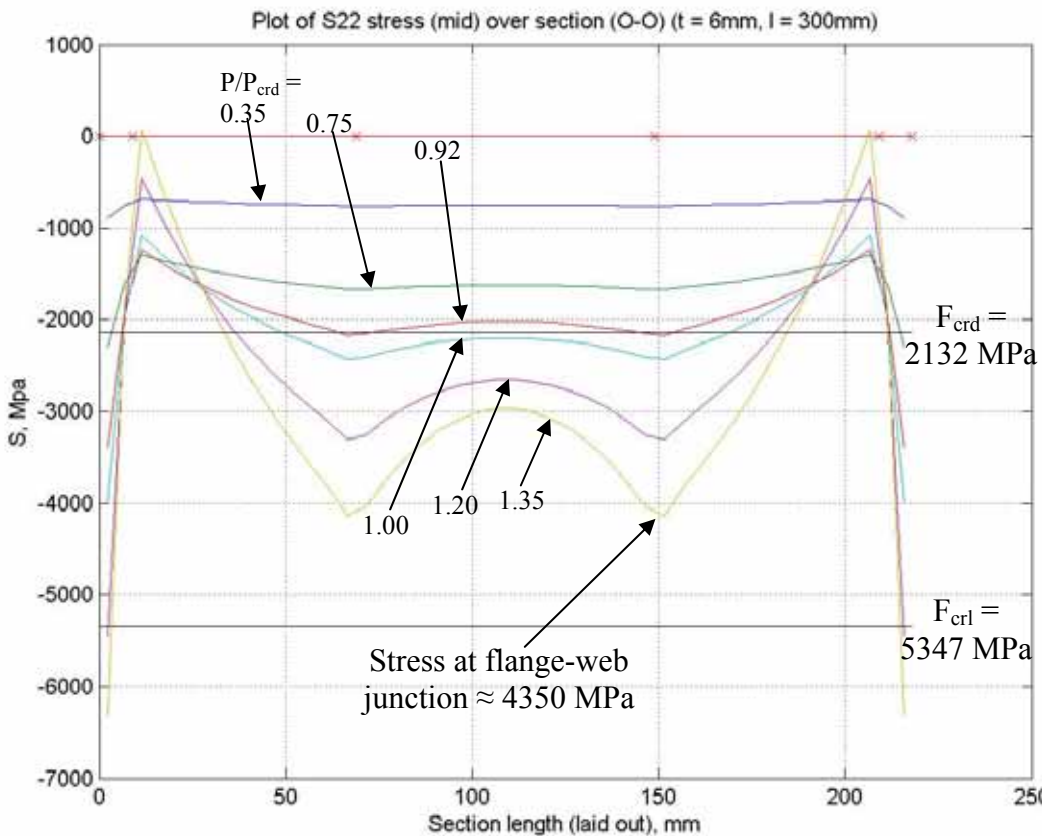


Figure 12 Plot of longitudinal stress distribution around section for t=6mm (O-O)

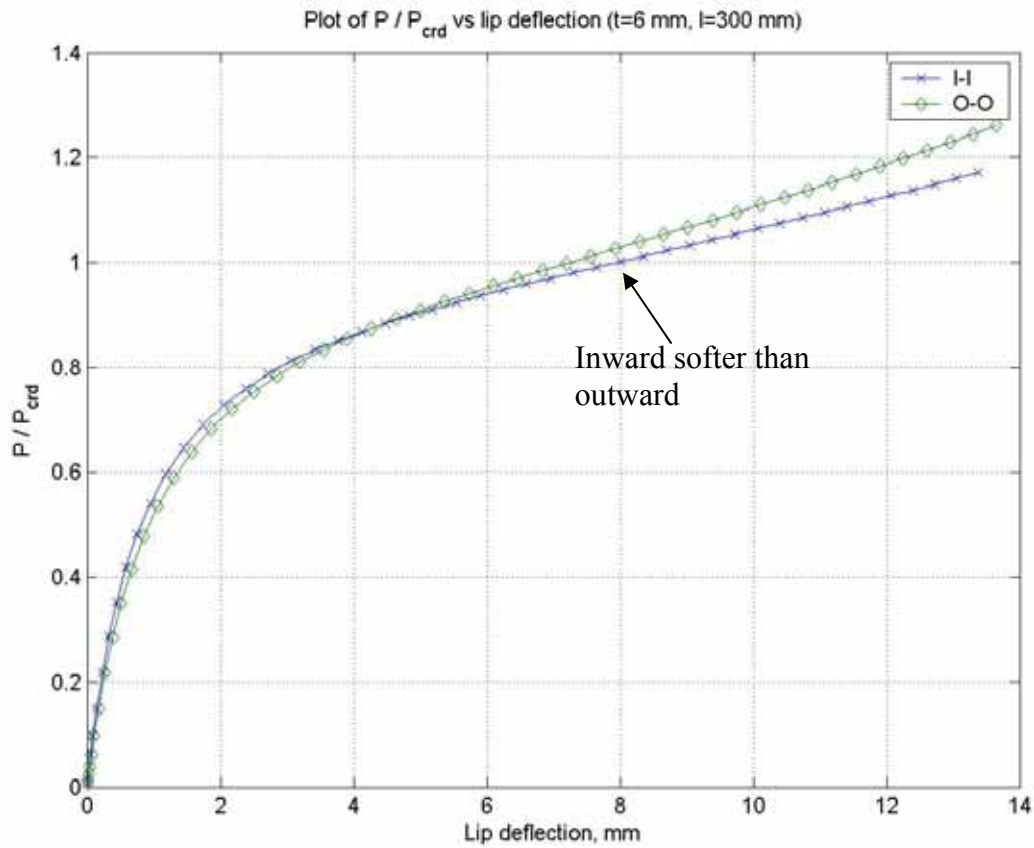


Figure 13 Plot of  $P/P_{crd}$  vs lip deflection for section  $t = 6$  mm

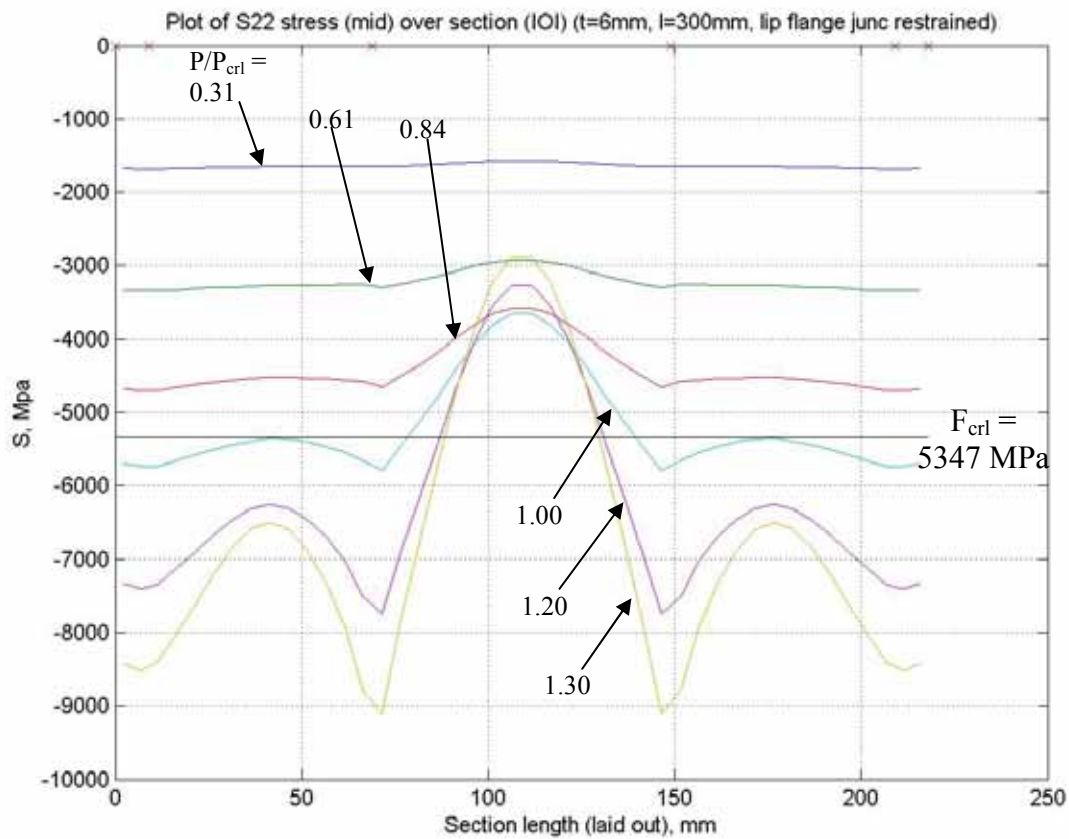


Figure 14 Plot of longitudinal stress distribution around section for  $t=6$  mm (forced local)

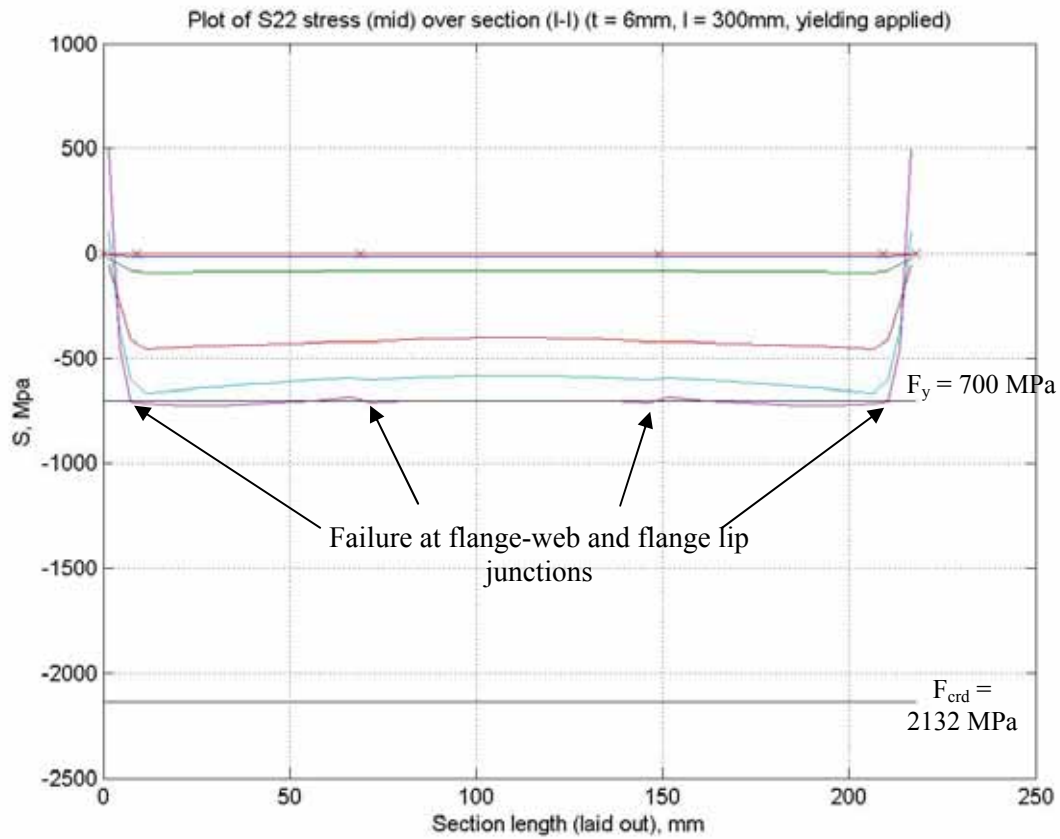


Figure 15 Plot of longitudinal stress distribution around section for  $t=6\text{mm}$  (I-I with yielding)

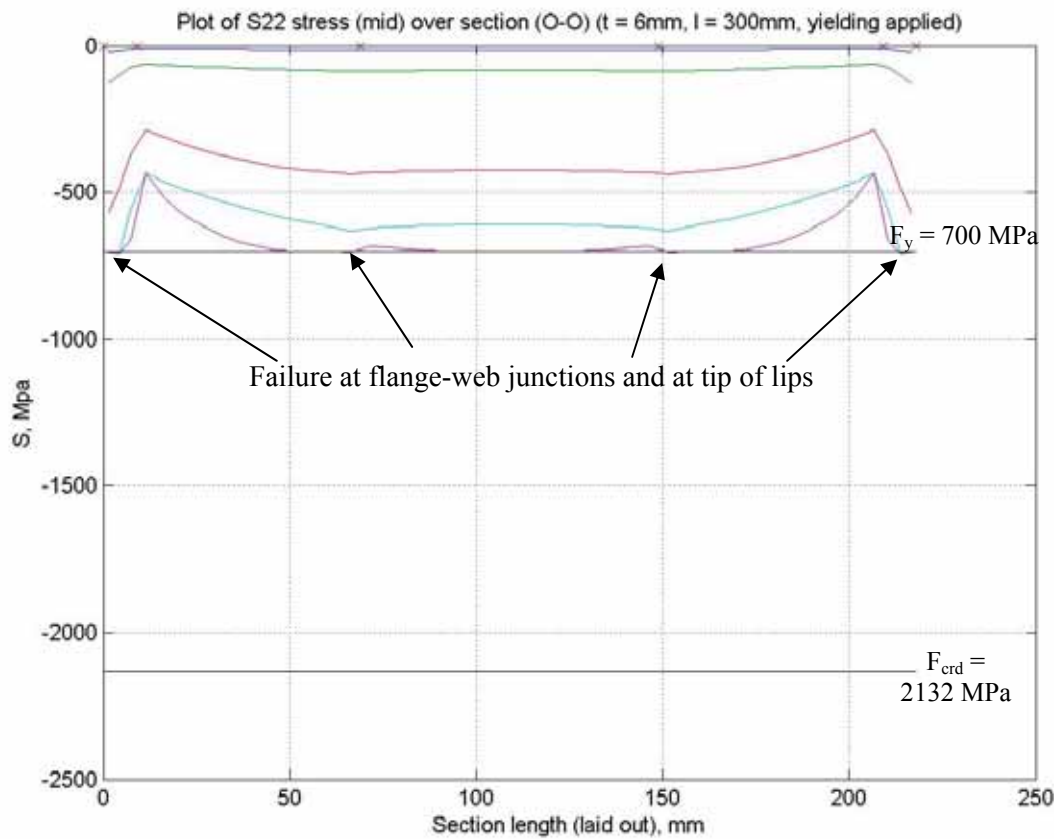


Figure 16 Plot of longitudinal stress distribution around section for  $t=6\text{mm}$  (O-O with yielding)

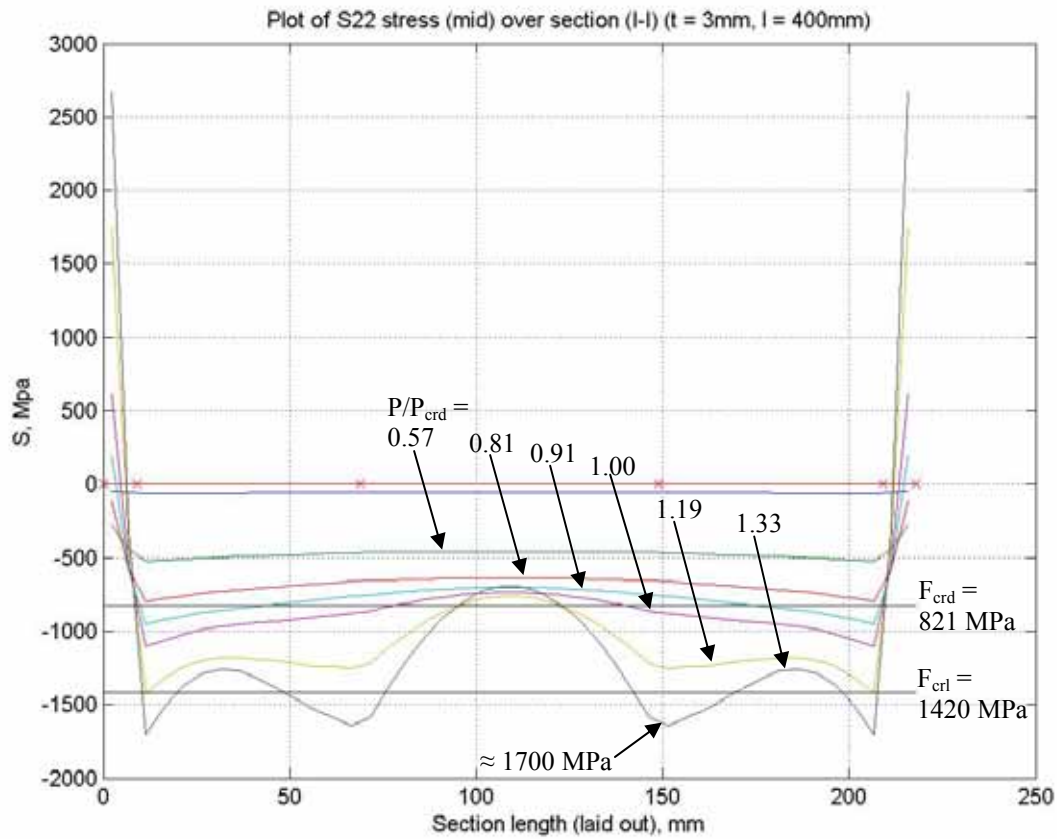


Figure 17 Plot of longitudinal stress distribution around section for  $t=3\text{mm}$  (I-I)

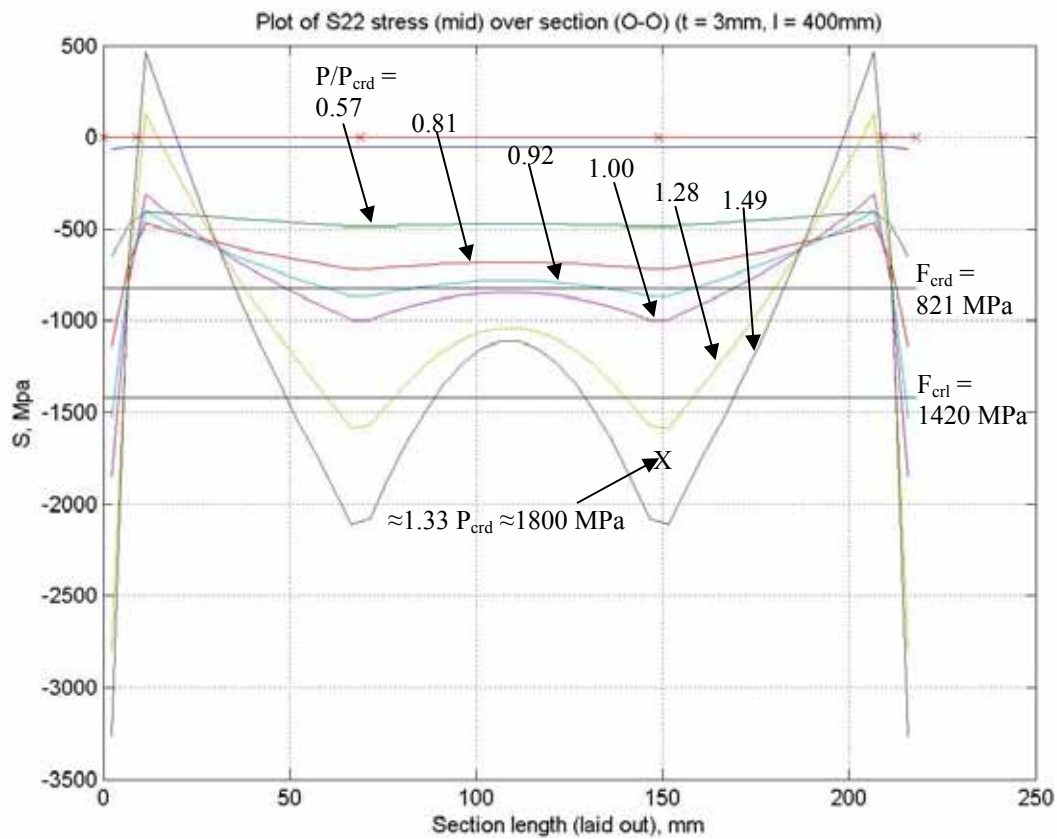


Figure 18 Plot of longitudinal stress distribution around section for  $t=3\text{mm}$  (O-O)

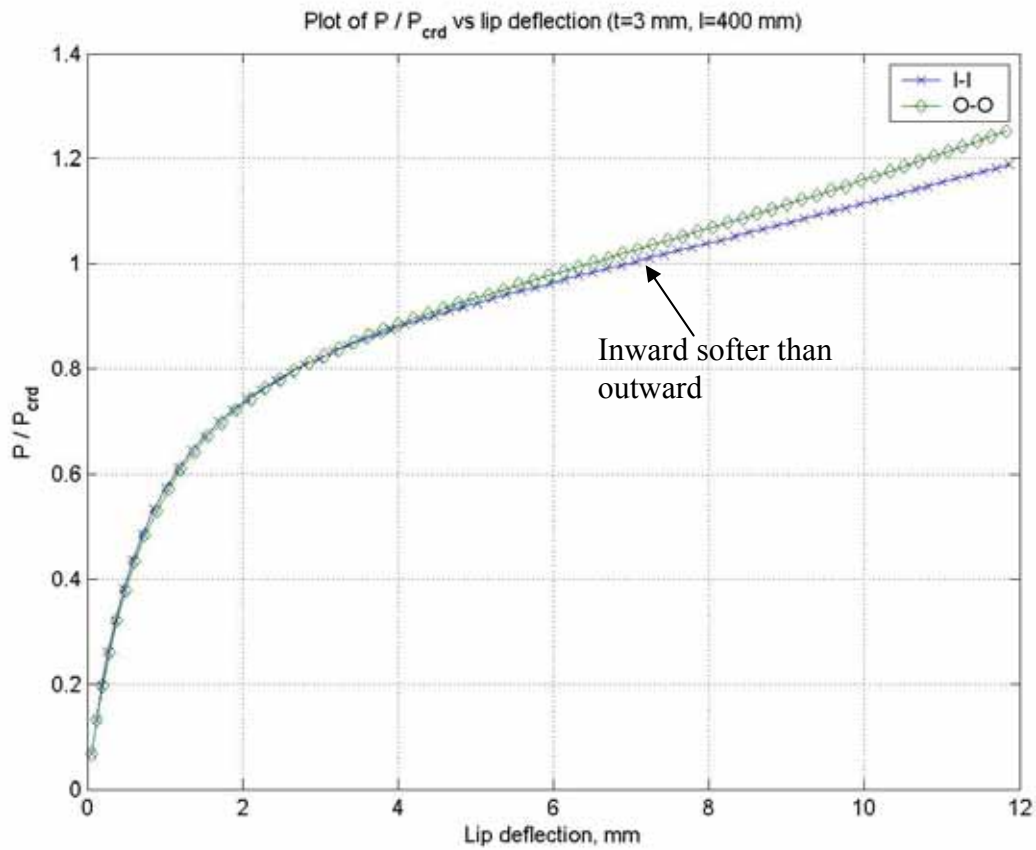


Figure 19 Plot of  $P/P_{crd}$  vs lip deflection for section  $t = 3\text{ mm}$

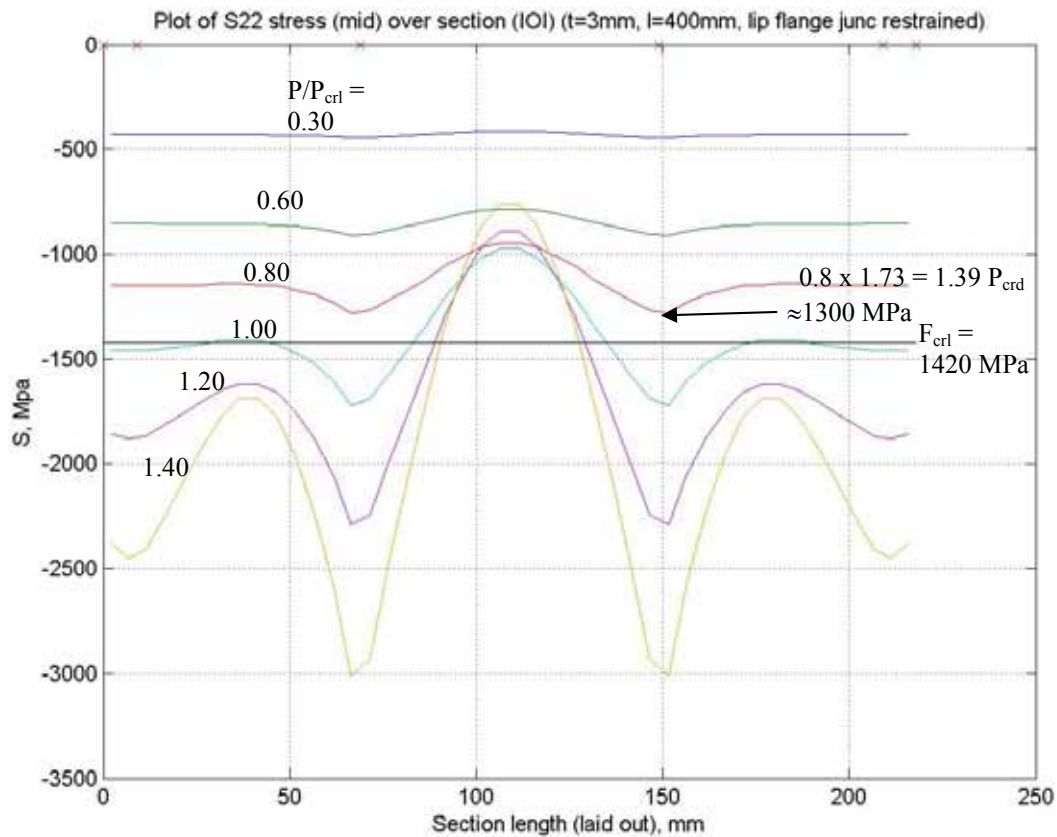


Figure 20 Plot of longitudinal stress distribution around section for  $t=3\text{ mm}$  (forced local)

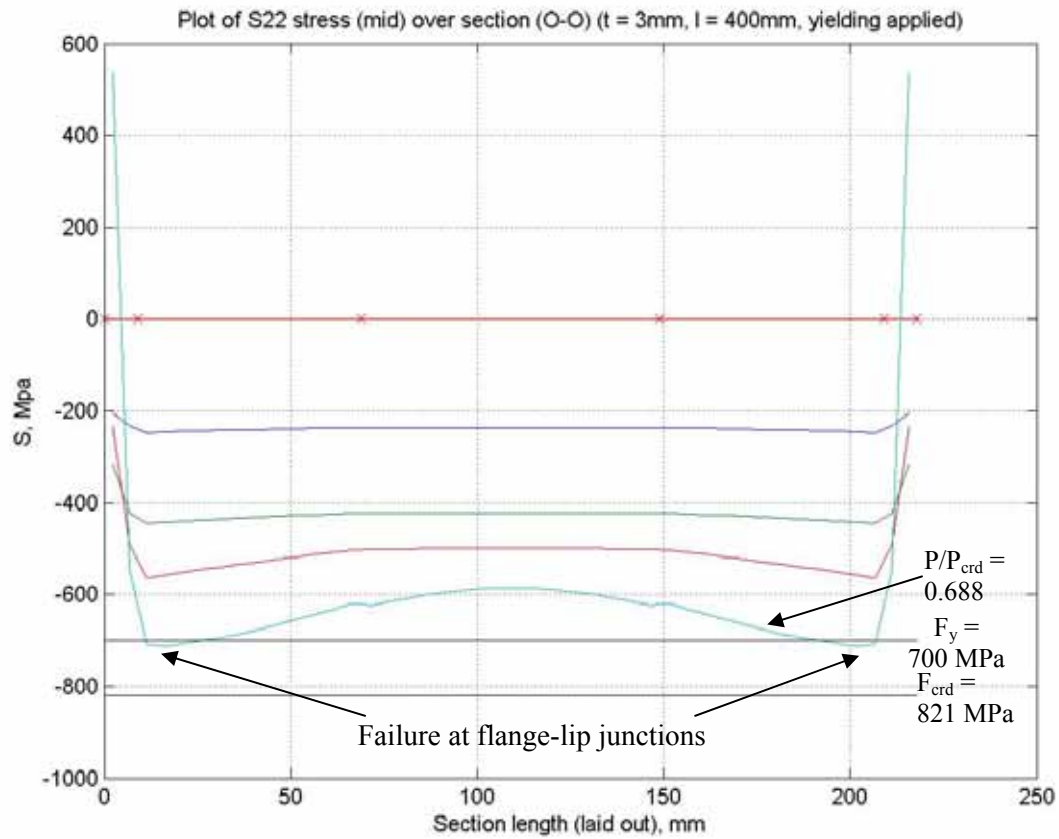


Figure 21 Plot of longitudinal stress distribution around section for  $t=3\text{mm}$  (I-I with yielding)

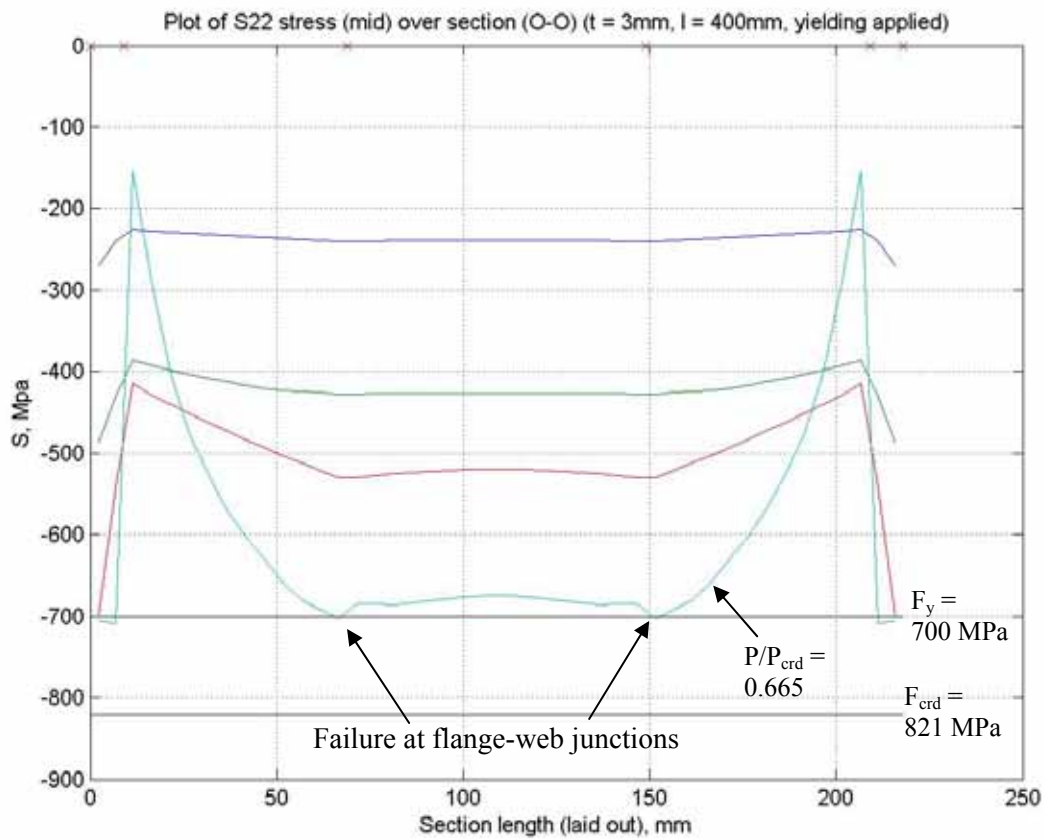


Figure 22 Plot of longitudinal stress distribution around section for  $t=3\text{mm}$  (O-O with yielding)

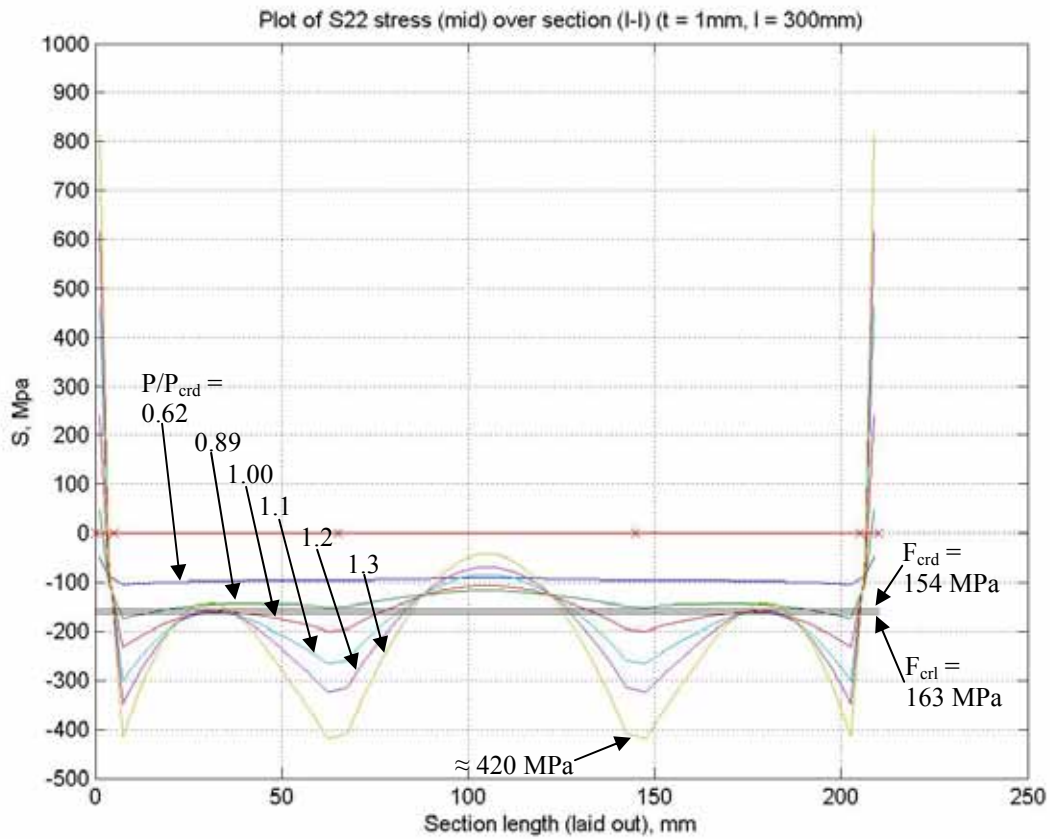


Figure 23 Plot of longitudinal stress distribution around section for  $t=1\text{mm}$  (I-I)

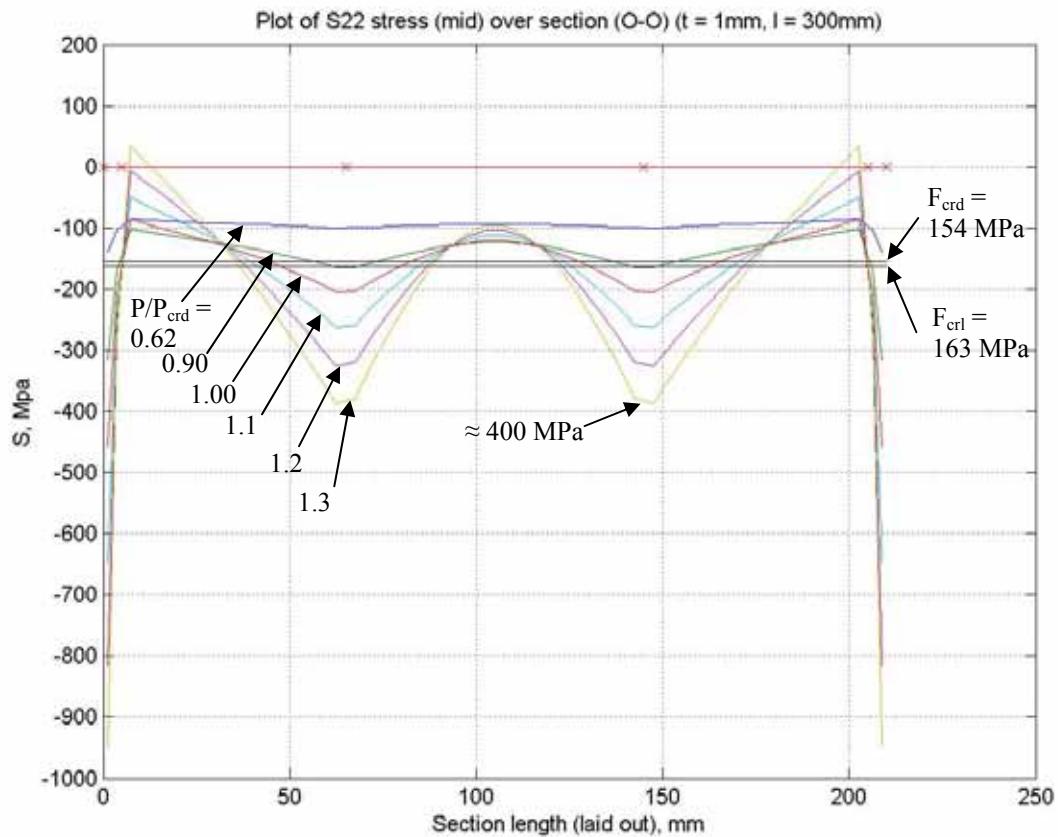


Figure 24 Plot of longitudinal stress distribution around section for  $t=1\text{mm}$  (O-O)

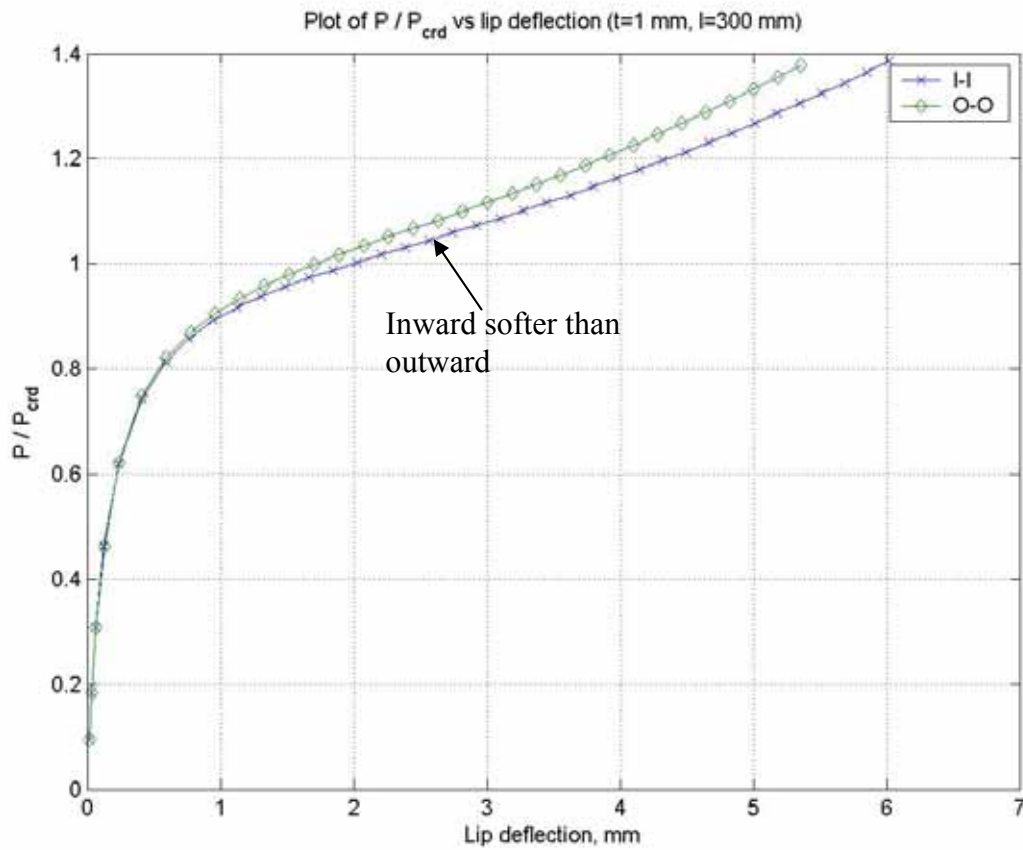


Figure 25 Plot of  $P/P_{crd}$  vs lip deflection for section  $t = 1$  mm

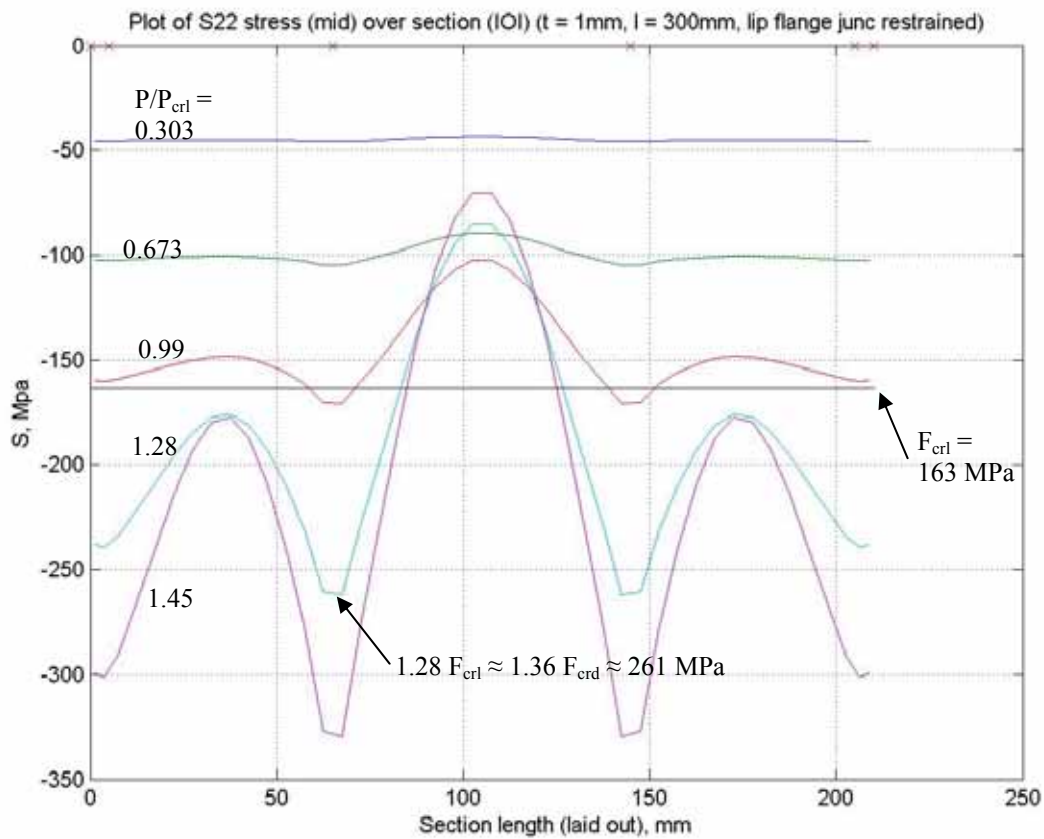


Figure 26 Plot of longitudinal stress distribution around section for  $t=1$ mm (forced local)

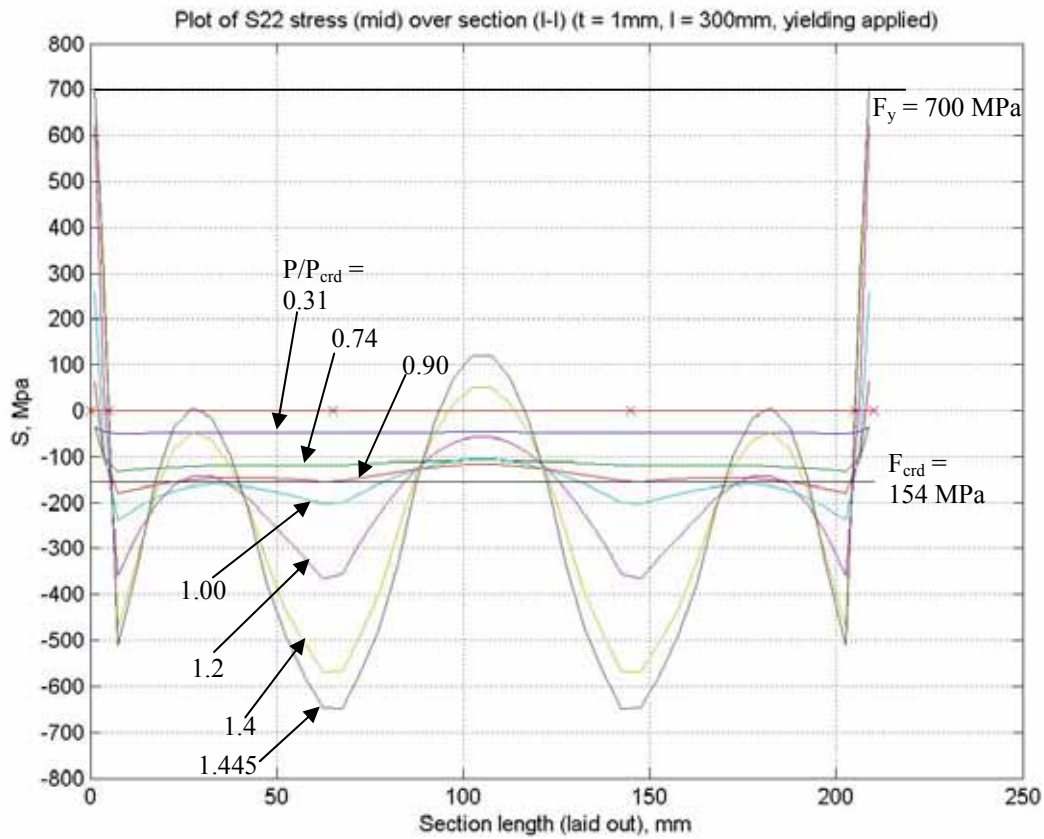


Figure 27 Plot of longitudinal stress distribution around section for  $t=1\text{mm}$  (I-I with yielding)

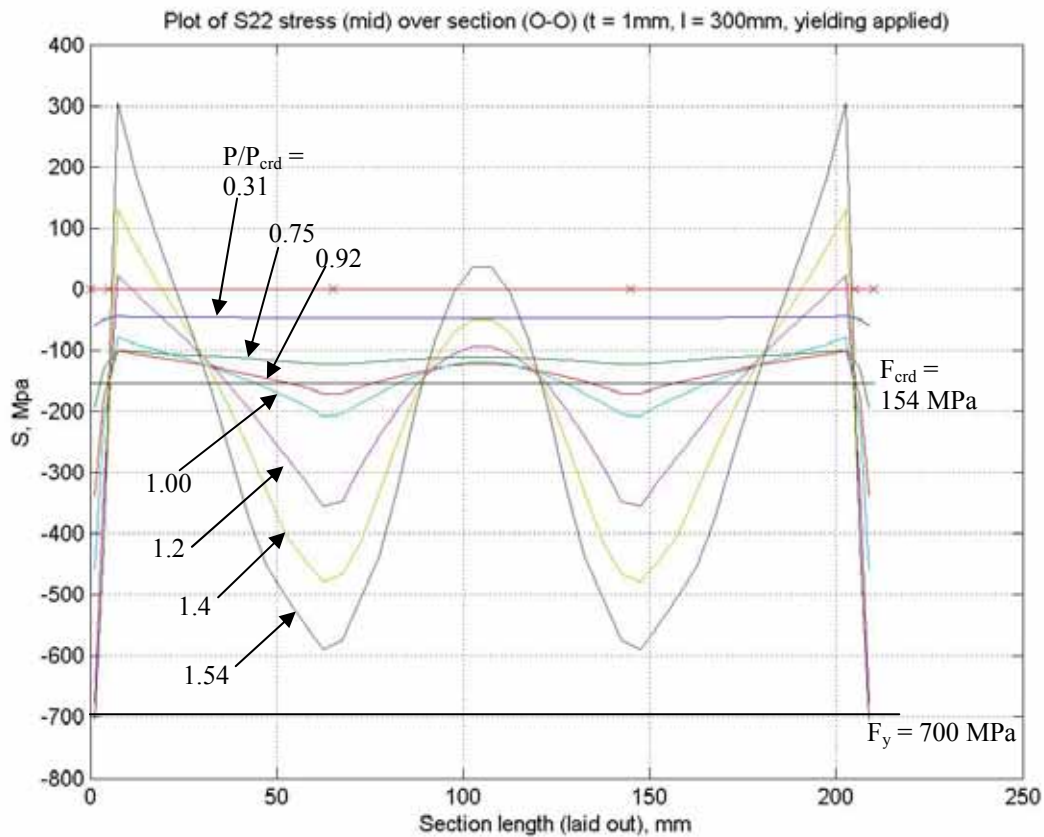


Figure 28 Plot of longitudinal stress distribution around section for  $t=1\text{mm}$  (O-O with yielding)

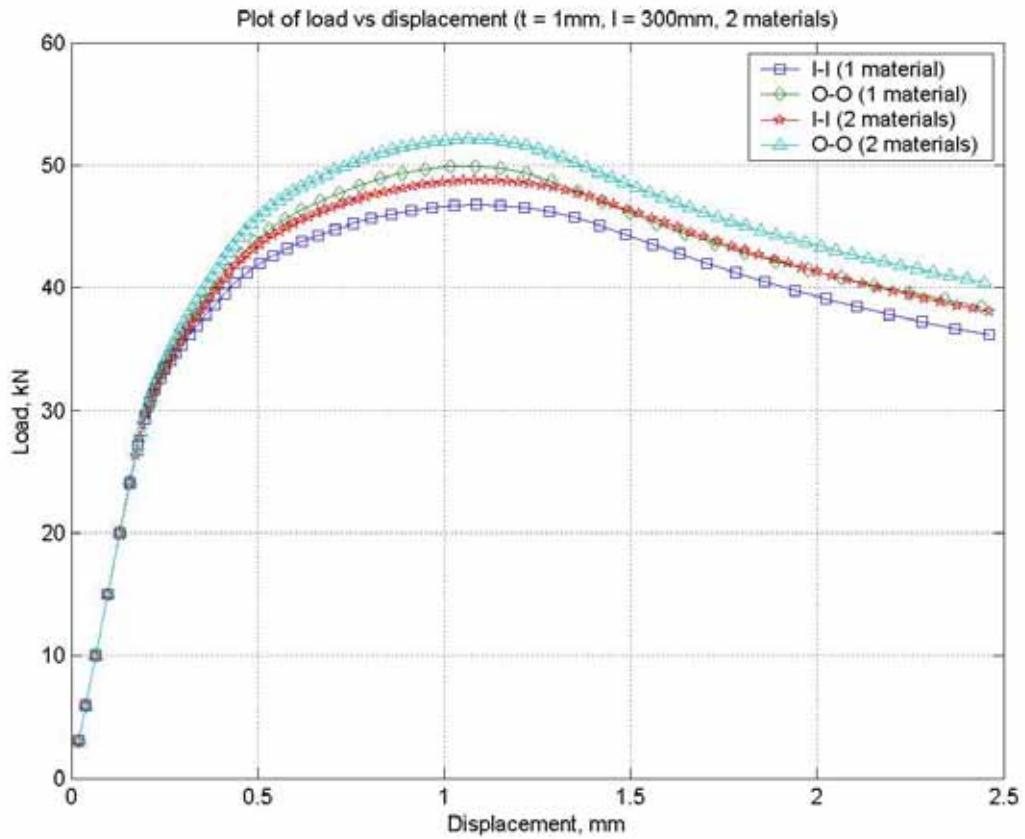


Figure 29 Plot of load vs displacement for  $t = 1 \text{ mm}$  (2 materials)

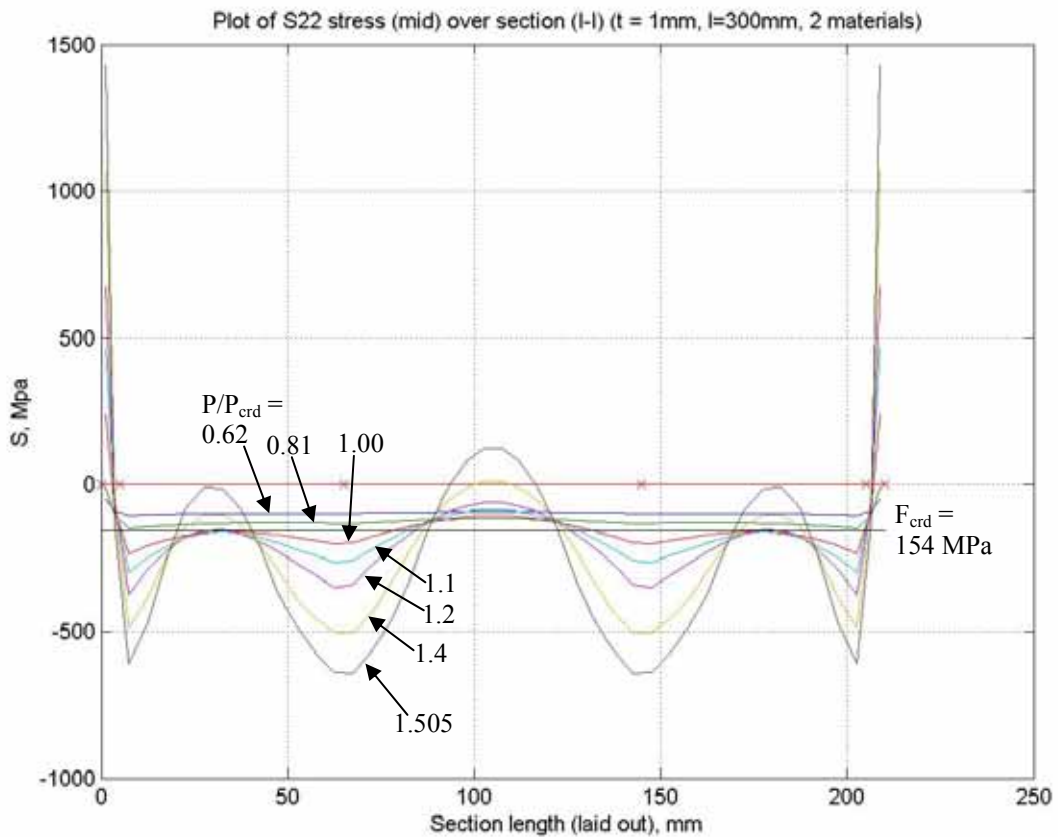


Figure 30 Plot of longitudinal stress distribution around section for  $t=1\text{mm}$  (I-I with 2 materials)

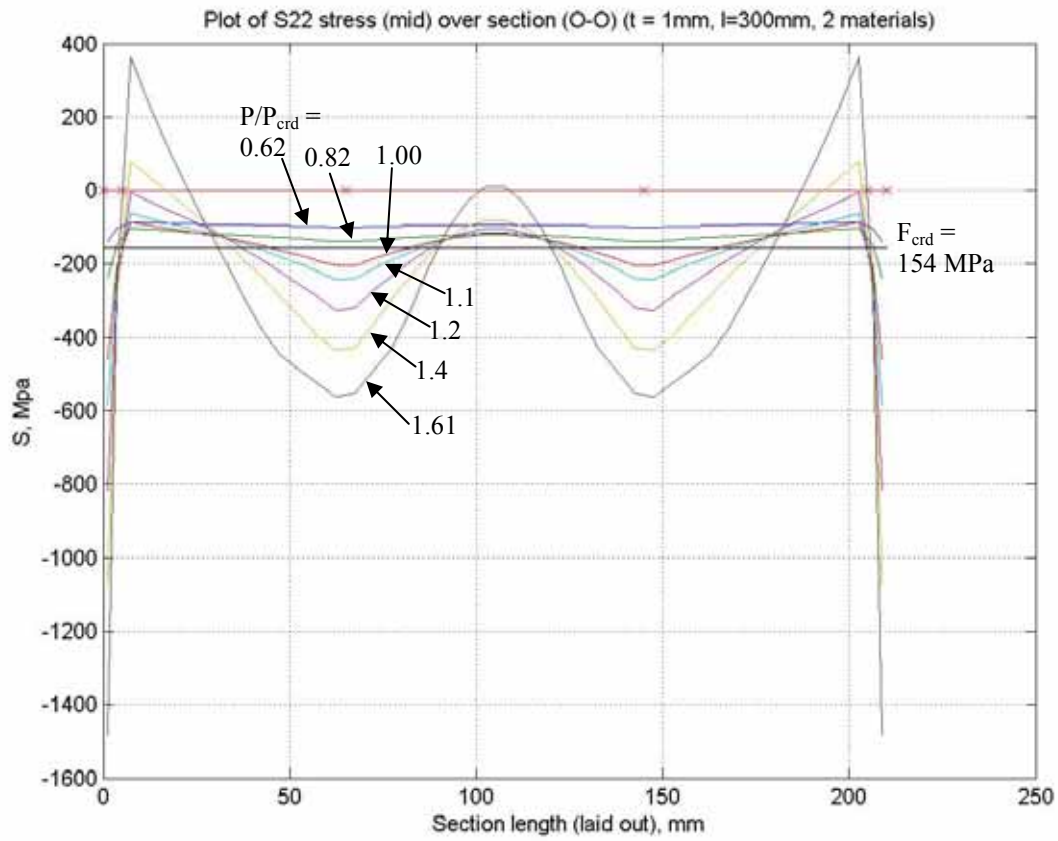


Figure 31 Plot of longitudinal stress distribution around section for t=1mm (O-O with 2 materials)

## TABLES

									% Difference between 0.64t and 0.15t						% difference wrt Kwon and Hancock strength equation (imperfection = $\pm 0.64t$ )			% difference wrt Kwon and Hancock strength equation (imperfection = $\pm 0.15t$ )		
t (mm)	A (mm <sup>2</sup> )	F <sub>y</sub> (MPa)	F <sub>crd</sub> (MPa)	P <sub>crd</sub> (kN)	Pu <sub>II</sub> (kN) 0.64t	Pu <sub>OO</sub> (kN) 0.64t	Pu <sub>II</sub> (kN) 0.15t	Pu <sub>OO</sub> (kN) 0.15t	(I-I)	(O-O)	Pu <sub>II</sub> /Py 0.64t	Pu <sub>OO</sub> /Py 0.64t	Pu <sub>II</sub> /Py 0.15t	Pu <sub>OO</sub> /Py 0.15t	% (II)	% (OO)	Average %	% (II)	% (OO)	Average %
6 (9mm lip)	1308	700	2133	2790	832.5	812.4	901.6	891.2	7.66	8.84	0.910	0.887	0.985	0.973	-9.08	-11.27	-10.17	-1.53	-2.67	-2.10
3 (9mm lip)	654	700	821.1	537.0	343.5	344.2	369.3	357.2	7.0	3.63	0.750	0.752	0.807	0.780	-8.08	-7.87	-7.97	1.13	-2.19	-0.53
2 (9mm lip)	436	700	605.8	264.1	171.9	179.4	195.7	192.8	12.4	7.05	0.563	0.588	0.641	0.632	-20.84	-17.40	-19.12	-9.25	-10.62	-9.94
2 (5mm lip)	420	700	333.5	140.1	155.2	166.4	157.0	167.9	1.13	0.86	0.528	0.566	0.534	0.571	-1.89	5.19	1.65	-0.77	6.11	2.67
1 (5mm lip)	210	700	154.2	32.38	46.24	49.31	46.79	49.91	1.17	1.21	0.314	0.335	0.318	0.340	-12.18	-6.37	-9.27	-12.26	-6.40	-9.33

Table 1 FEA distortional buckling results compared to design strength curves for distortional buckling

Thickness	$F_{cr1}$ (MPa)	$P_{cr1}$ (kN)	$\frac{P_{cr1}}{P_{crd}}$	$P_{u_{local}}$ (kN)	% difference wrt Winter strength equation
<b>6 mm (9 mm lip)</b>	5347	6993.9	2.51	-	-
<b>3 mm (9 mm lip)</b>	1420	928.7	1.73	428.0	-4.41
<b>2 mm (9 mm lip)</b>	649.9	283.3	1.07	235.6	1.67
<b>2 mm (5 mm lip)</b>	647.4	271.9	1.94	224.5	0.71
<b>1 mm (5 mm lip)</b>	163.6	34.36	1.06	67.94	6.98

**Table 2 Local buckling stresses and ultimate loads**